Liquid repellent surfaces

Stephen Richard Coulson

Group	Vibrational Mode	Wavenumber / cm^{-1}		
		Literature [41]	**Monomer**	**Pulsed Plasma Polymer**
Ester C=O	stretching	1750-1715	1734	1736
Acrylate	s-trans and s-cis rotational isomers	1640 & 1625	1640 & 1625	not seen
Acrylate	$=CH_2$ in plane deformation	1420-1410	1412	not seen
$-CF_3$	stretching	1350-1120	1236-1117	1196-1117
Acrylate	CH in plane deformation	1300-1290	1298	not seen
$-CF_2-$	stretching	1280-1120	1236-1117	1196-1117
Acrylate	CH out of plane deformation	995-985	986	weak
Acrylate	$=CH_2$ wag	965 ± 5	970	weak
Acrylate	$=CH_2$ twist	811 ± 3	812	not seen

Table 2.3 Infrared absorption band assignments.

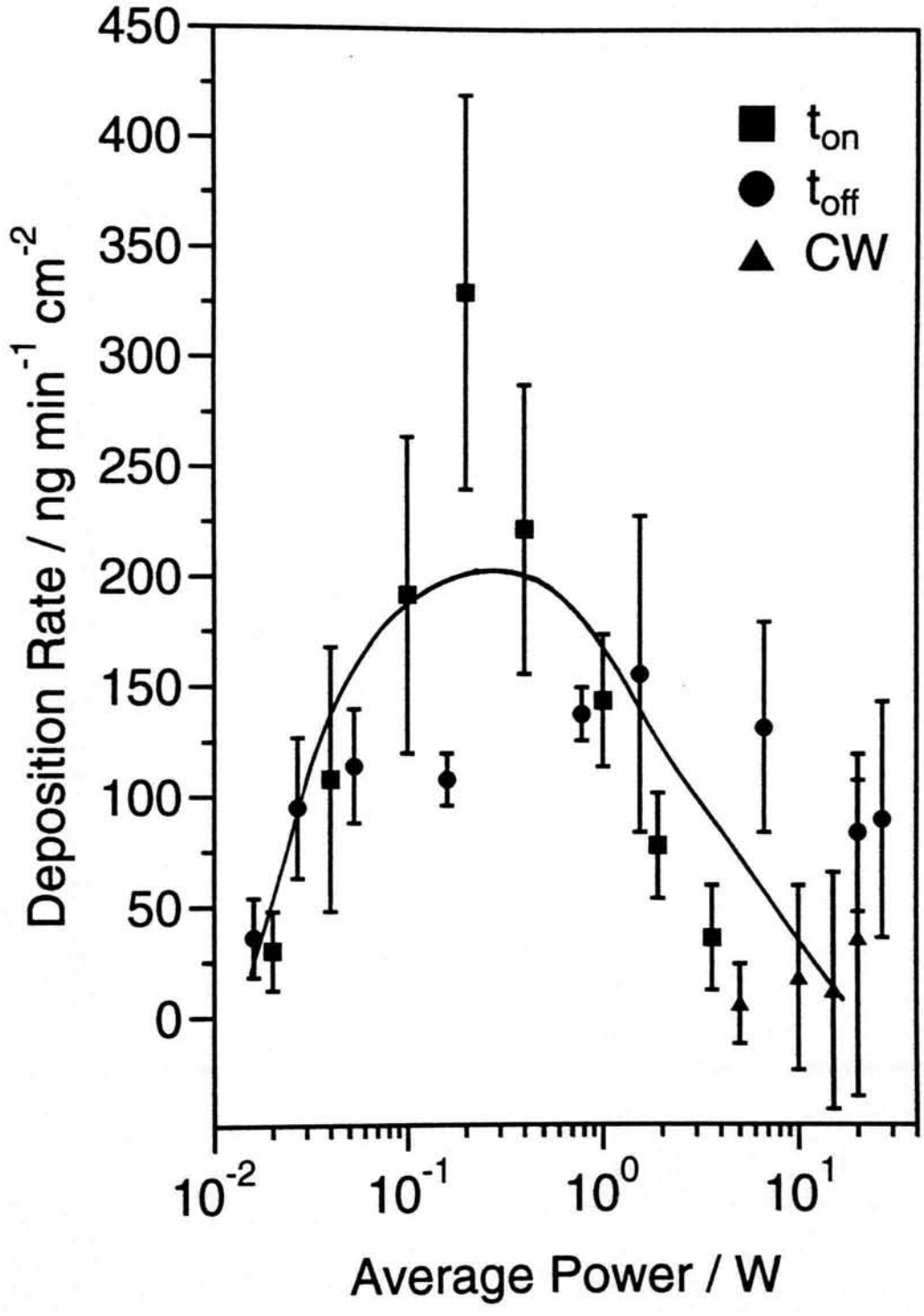

Figure 2.5a Influence of average power upon deposition rate.

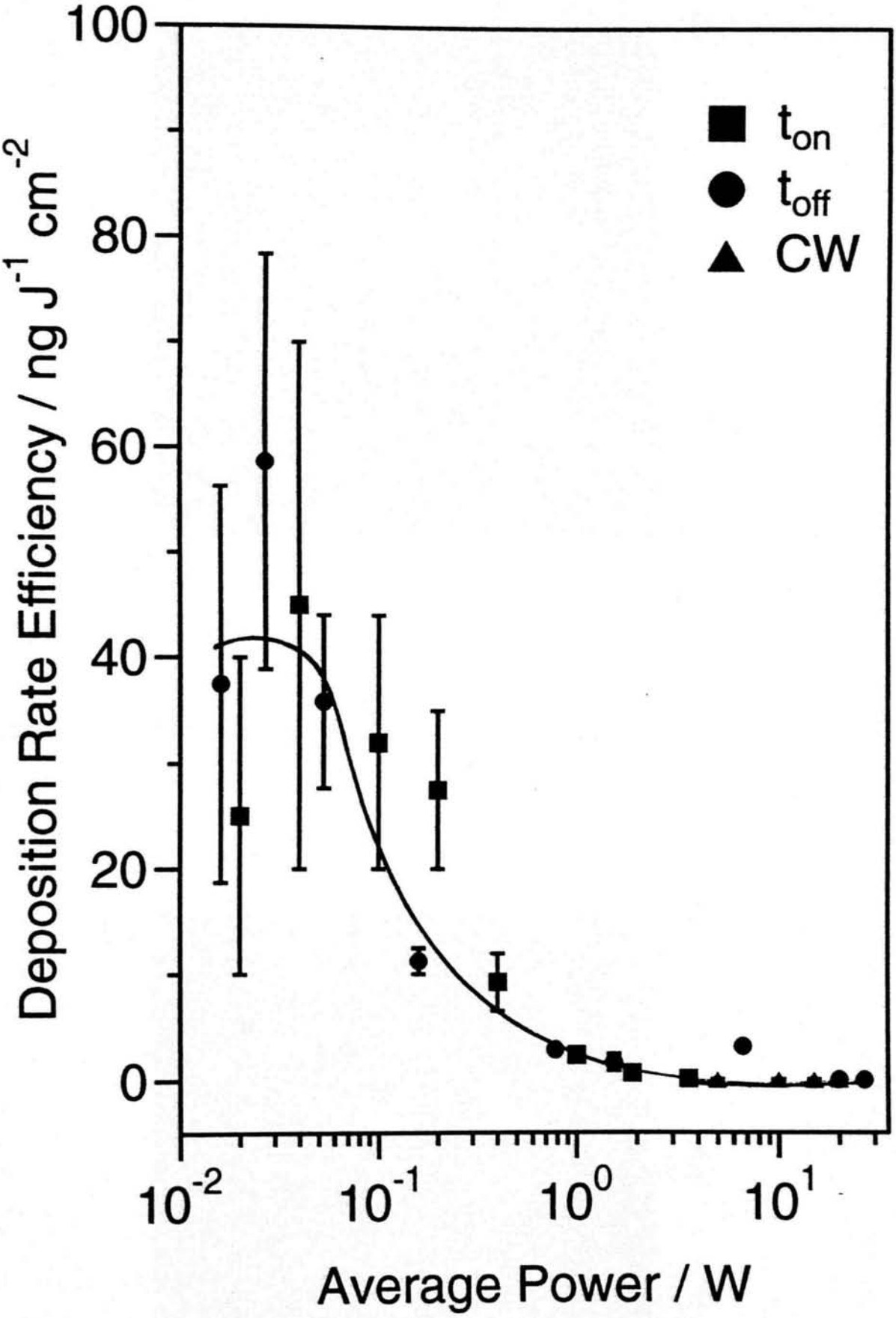

Figure 2.5b Influence of average power upon deposition rate efficiency.

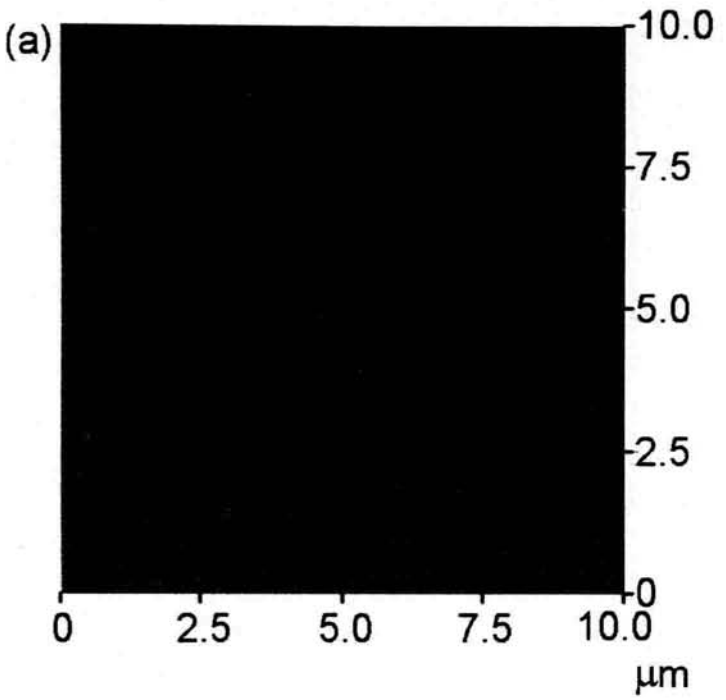

Figure 2.6a AFM micrograph of a clean glass substrate.

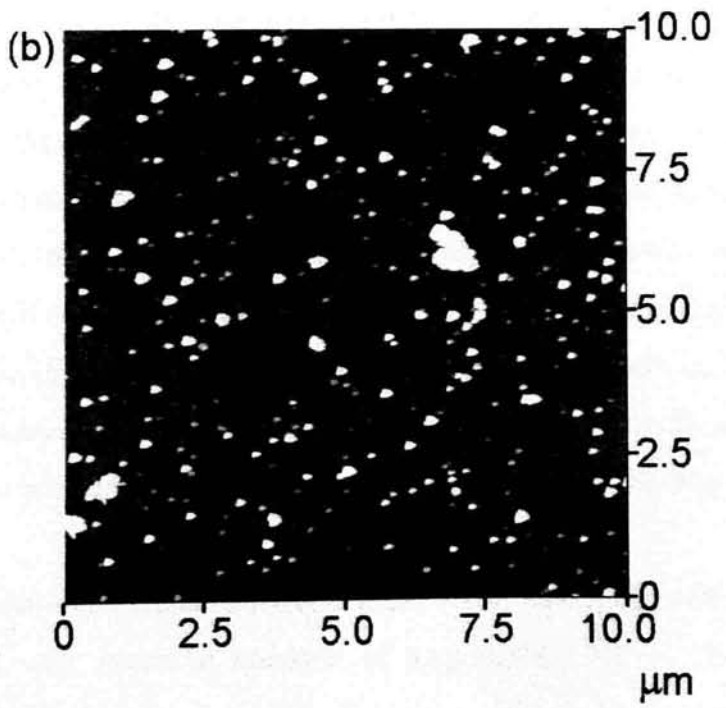

Figure 2.6b AFM micrograph of a 5 W continuous wave plasma polymer film of 1H,1H,2H,2H-heptadecafluorodecyl acrylate.

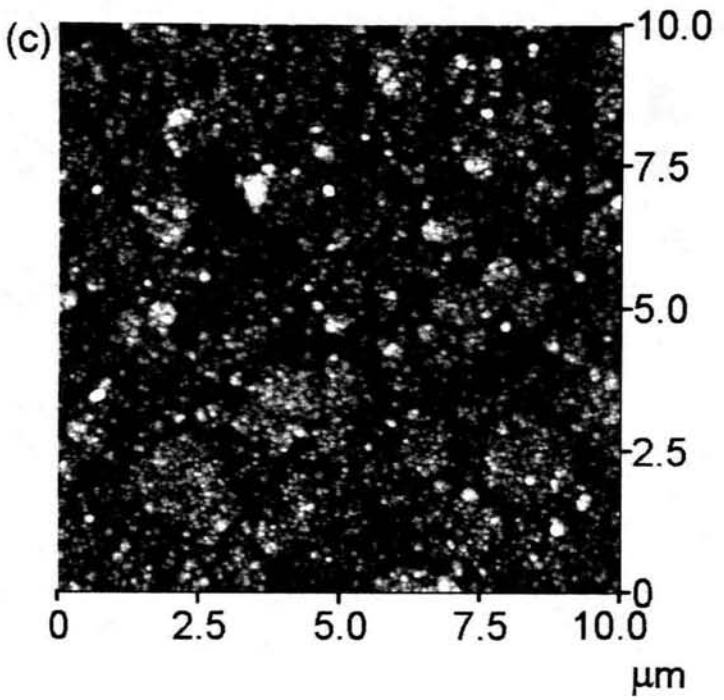

Figure 2.6c AFM micrograph of a pulsed plasma polymer film of 1H,1H,2H,2H-heptadecafluorodecyl acrylate (t_{on} = 20µs, t_{off} = 20,000 µs, P_p = 40 W).

Short pulse duty cycles gave rise to a drop in surface energy, eventually reaching a limiting value of 10 mN m^{-1} (measured by the combined geometric mean-Young's equation), Figures 2.7a and 2.7b. Comparison with Figure 2.3 shows that the polar contribution disappears with increasing structural retention of the perfluoroalkyl chains. The absence of any polar contribution to the total surface energy under these conditions meant that it was valid to use a homologous series of alkane probe liquids to make a Zisman plot [6]. Critical surface tension values of γ_c = 4.3 mN m^{-1} and γ_c = 14.4 mN m^{-1} were obtained for optimum pulsed (t_{on} = 20 µs, t_{off} = 20,000 µs, P_p = 40 W) and continuous wave (5 W) plasma polymer coatings respectively, Figures 2.8a and 2.8b.

The extremely low critical surface tension value measured in the former case can be associated with structural retention of long perfluoro-alkyl chains at the air-solid interface.

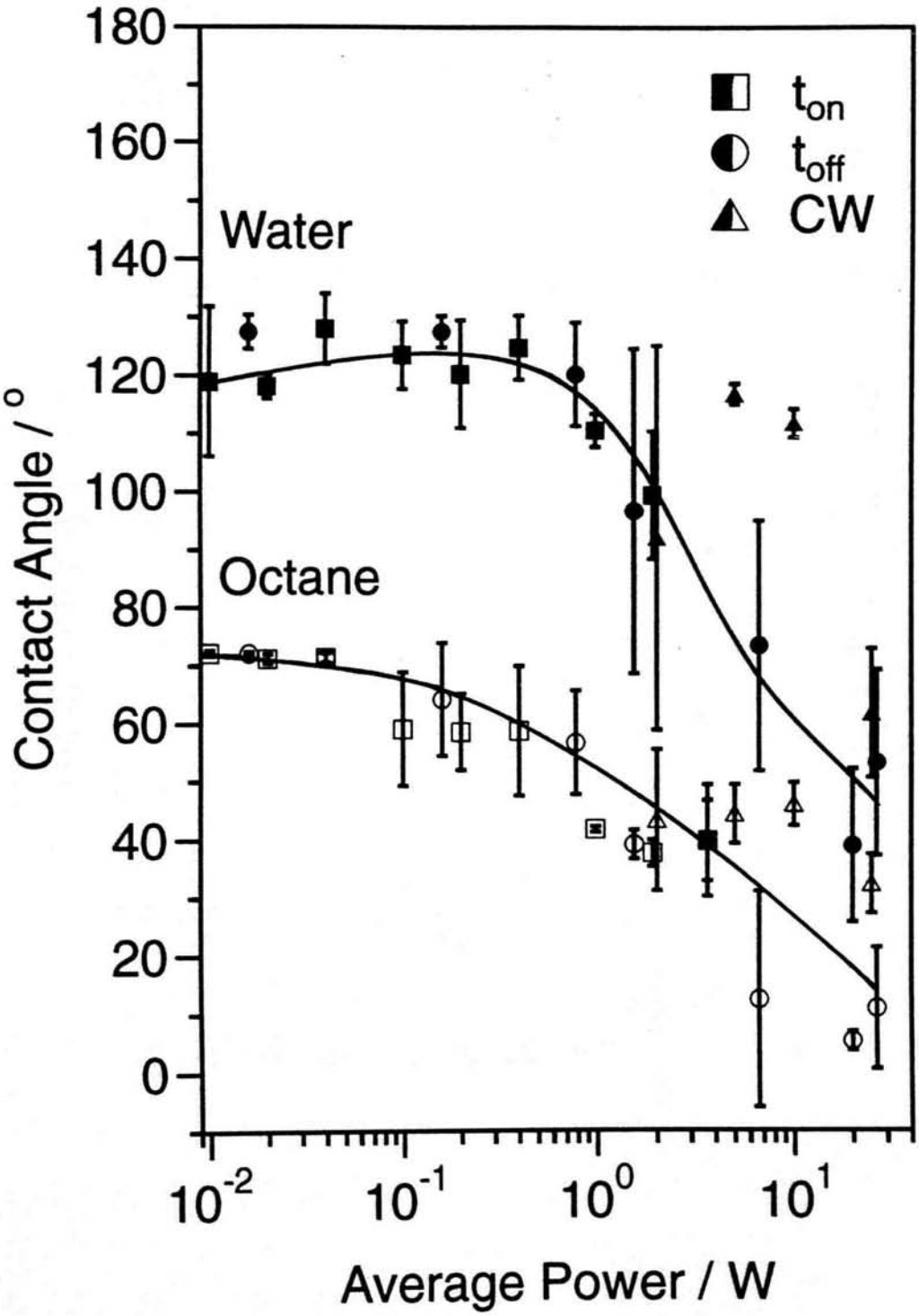

Figure 2.7a Influence of average power upon water (shaded) and octane (unshaded) advancing contact angles.

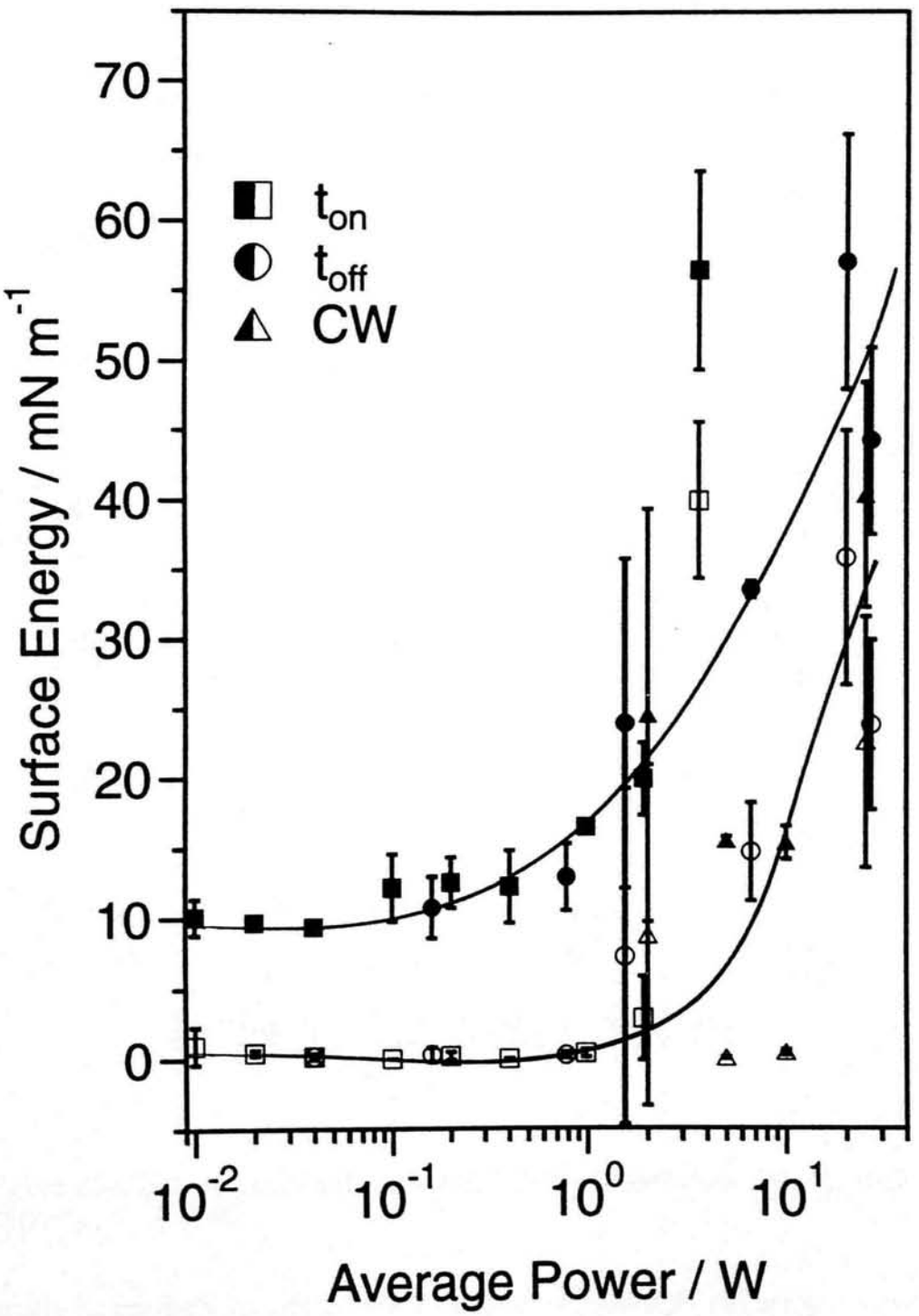

Figure 2.7b Influence of average power upon surface energy values calculated using combined geometric mean-Young's equation, where the unshaded symbols correspond to the polar component and the shaded ones are the total surface energy.

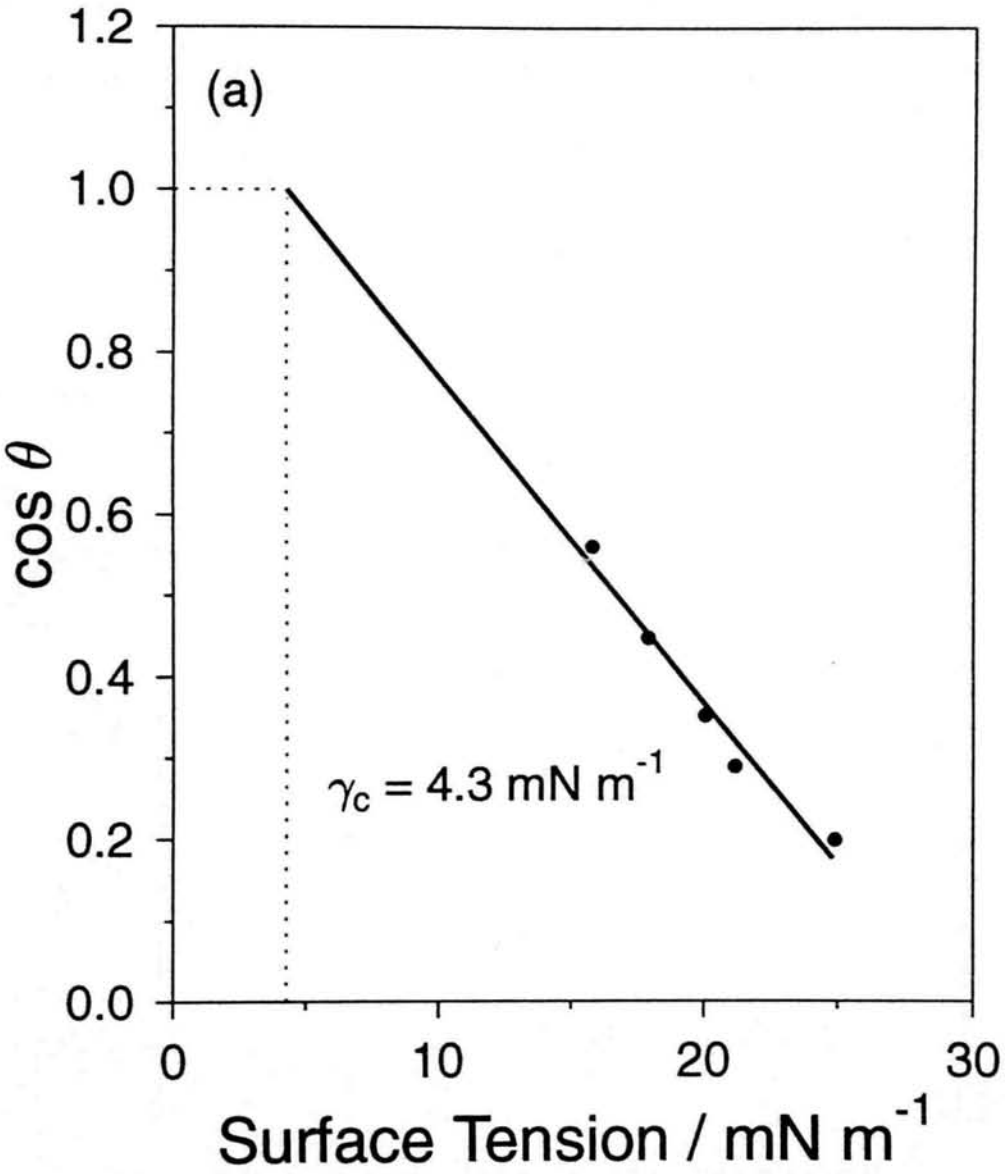

Figure 2.8a Zisman plot of pulsed plasma polymer coated glass slide (t_{on} = 20 μs, t_{off} = 20,000 μs, P_p = 40 W).

Finally, hydrophobicity and oleophobicity tests were carried out using a range of pure liquids and water / isopropyl alcohol mixtures with differing surface tensions [42], Table 2.1. This comprised placing 3 drops of each test liquid onto coated cotton fabric. The surface was considered to repel each liquid if after 30 s (for oleophobicity and 10 s for hydrophobicity), the drops remained spherical / hemispherical, i.e. absence of any penetration or wicking at the liquid-fabric interface. 5 W continuous wave plasma deposited coatings were found to be repellent only towards 40% water / 60%

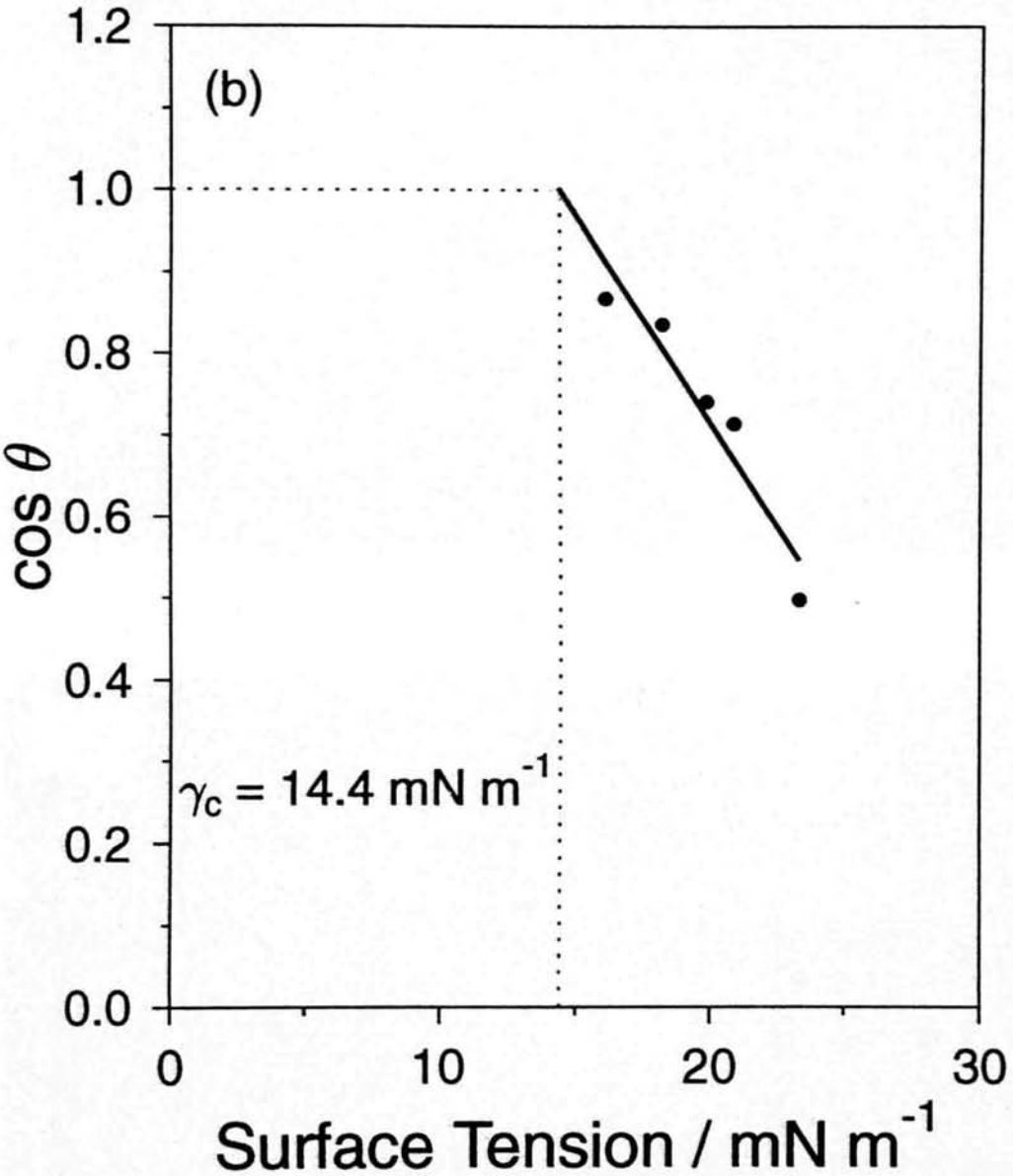

Figure 2.8b Zisman plot of 5 W continuous wave plasma polymer coated glass slide.

isopropyl alcohol mixtures and dodecane, higher concentrations of isopropyl alcohol and shorter alkane chains wetted the substrate. A significant improvement was noted for optimum pulsed plasma deposition conditions, where liquid repellency was observed towards pure isopropyl alcohol as well as water (hydrophobicity), and also alkane chains as short as heptane (oleophobicity), Figure 2.9.

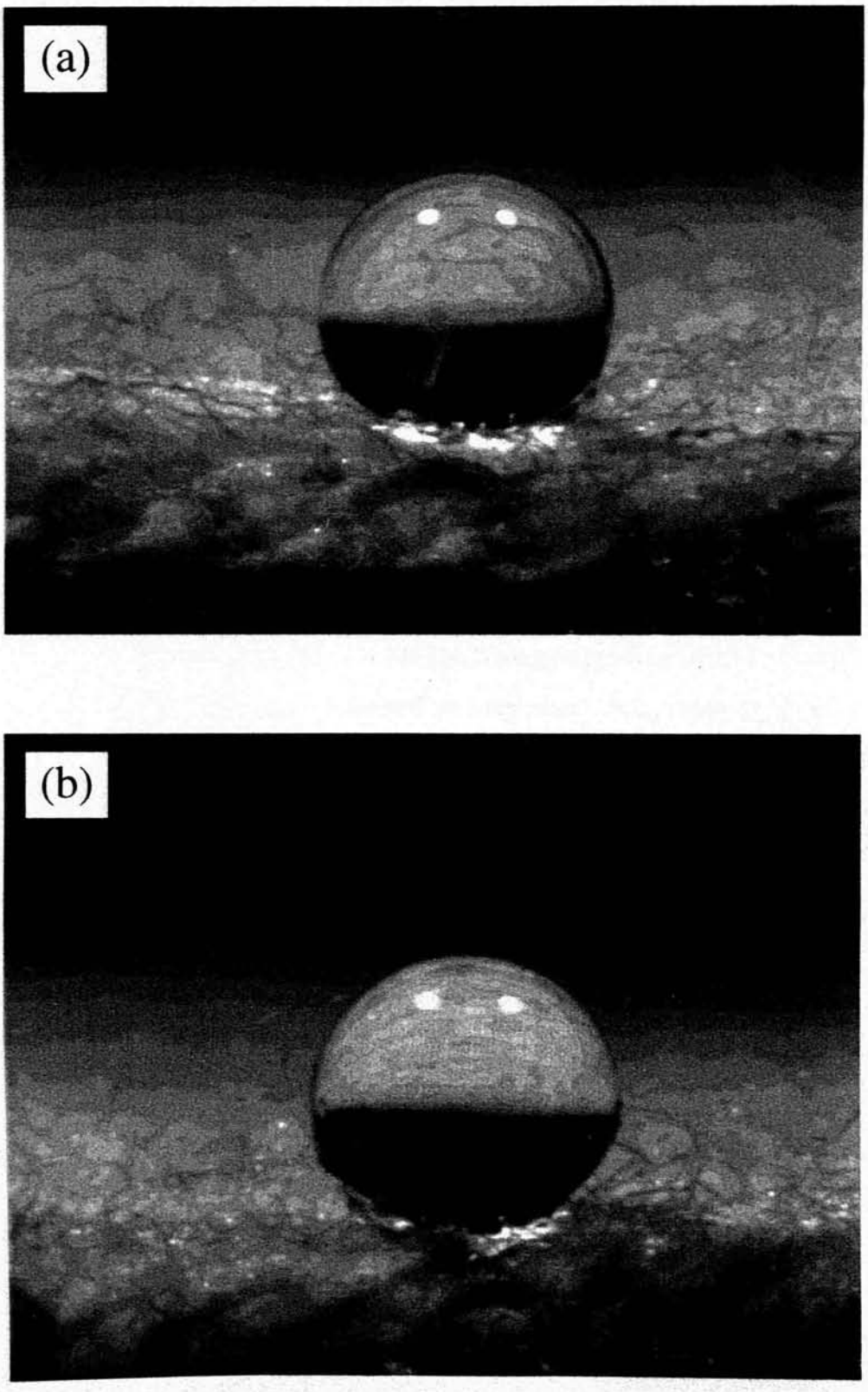

Figure 2.9 Optical images illustrating liquid repellency (2 µl droplet volume) for 1H,1H,2H,2H-heptadecafluorodecyl acrylate pulsed plasma polymer layer deposited onto cotton fabric (t_{on} = 20 µs, t_{off} = 20,000 µs, P_p = 40 W): (a) pure isopropyl alcohol droplet; and (b) heptane droplet.

2.4. *DISCUSSION*

The described plasma polymerisation method is quick, cheap, substrate-independent, solventless, does not require additional non-fluorochemical reagents (e.g. catalysts, crosslinking agent, surfactants, etc. [10]) and therefore a cleaner fluoropolymer product can be expected. The greater retention of $>\underline{C}F_2$ groups observed during electrically pulsed plasma polymerisation compared to continuous wave conditions is consistent with less fragmentation and damage of the perfluoroalkyl tail, Table 2.2. This can be attributed to a drop in plasma sheath potential, causing less energetic ion bombardment of the growing film [43] and attenuation of VUV irradiation [44].

Normally deposition rate is found to increase with rising average power for continuous wave conditions [18]. However a reversal in this trend occurred during pulsed plasma polymerisation of 1H,1H,2H,2H-heptadecafluorodecyl acrylate, Figure 2.5a. Poor deposition rates measured at very short duty cycles can be ascribed to the lack of polymerisation sites. A maximum is reached at intermediate pulse cycles, corresponding to the highest ratio of polymerisable species to non-polymerisable / ablative species. Upon approaching continuous wave conditions, the deposition rate drops as a consequence of ablation becoming a competing process. In order to factor out the effect of variation in average power, the deposition rate efficiency was calculated (defined as deposition rate divided by average power) [45], Figure 2.5b. It is found that the deposition rate per joule of energy increases with decreasing average power. This can be taken as being indicative of species which are activated during the on-period (via UV irradiation, ion or electron bombardment etc.) polymerising via conventional free radical pathways. This can occur either in the gas phase or at the plasma-substrate interface, during the off-period of the pulse cycle.

Most previous studies have utilised the Zisman method to assess low critical surface tension coatings. The critical surface tension values, γ_c, measured for solution phase polymerised 1H,1H,2H,2H-heptadecafluorodecyl acrylate and other long chain

perfluoroacrylates and methacrylates can be as low as 10 mN m^{-1} [10], [11], [40], [46], [47]. In fact, the lowest γ_c value mentioned in the literature is 6 mN m^{-1} for a monomolecular layer of $CF_3(CF_2)_{10}CO_2H$ [7], [9]. Lower critical surface tensions

have been hinted at, however no values have been reported [48]. It appears that the value of γ_c = 4.3 mN m^{-1} attained in the present case for the pulsed plasma polymer coatings is comparable. The errors for the mean values plotted on the Zisman plots are ± 0.06. It should be noted that the data could also be fitted with a curve, giving a critical surface tension of $\gamma_c = 7 \pm 3$ mN m^{-1} for the pulsed plasma polymer coating, comparable to the surface energy data obtained using the geometric mean method. All previous data represented in this manner was fitted using a straight line [10], [11], [40], [46], [47] and hence the method used here. From raw data values it is clear that the contact angles obtained here are greater then those reported. The micro-roughness discernible in the AFM micrographs could potentially distort the Zisman plot to give anomalous γ_c values.

If the roughness causes air to become trapped in the voids (i.e. the liquid cannot penetrate into the troughs), then a composite interface will be formed in accordance with the Cassie-Baxter relationship [49]. In fact this is how high water repellency has been achieved in the past for powdered plasma polymer films [21], [50], [51], [52], [53]. However such behaviour appears to be unlikely, since the low contact angle hysteresis normally associated with a composite interface [21], [54] is absent for the pulsed plasma polymer layers (advancing and receding contact angle values, θ_{adv} / θ_{rec} = 134° / 66° and 74° / 35° for water and octane respectively). The observed contact angle hysteresis is more consistent with the surface roughness only being sufficient to produce an effective increase in surface area without pore formation. This can be described in terms of Wenzel's law [21], [50], [55], [56], which predicts that surface roughening decreases / increases the repellency of liquids which make a contact angle of less / greater than 90° on the corresponding flat surface. In the present case, any distortion in the critical surface tension value to an abnormally small value due to a consequence of surface roughness is unlikely, since the chosen series of low surface tension alkane probe liquids all exhibit contact angles less than 90°. According to Wenzels law [55], surface roughness will actually make the measured liquid contact angle lower than the true value [57], [58], hence $cos\theta$ will be greater for each probe liquid on the Zisman plot; thereby shifting the measured γ_c value artificially higher.

2.5. *CONCLUSIONS*

Pulsed plasma polymerisation is an effective method for the functionalisation of solid surfaces. Short duty cycle on-times in conjuncti off-times enable selective activation of reactive bonds contained within Precursors containing long perfluoroalkyl chains (e.g. 1H heptadecafluorodecyl acrylate), yield low surface energy coatings, w excellent repellency towards low surface tension liquids.

2.6. *REFERENCES*

[1] B. Boutevin, Y. Pietrasanta in *Les Acrylates et Polyacrylates Fluorés: Dérivés et Applications* EREC, Paris, **1988**.

[2] L. Klinger, J. R. Griffith, *Org. Coat. Appl. Polym. Sci.* **1983**, *48*, 407.

[3] C. Bonardi, *Eur. Patent Appl.* EP 426,530, Elf Atochem, inv. **08.05.91**.

[4] C. G. DeMarco, A. J. Macquade, S. J. Kennedy, *J. Mod. Text. Mag.* **1960**, *2*, 50.

[5] M. K. Bernett, W. A. Zisman, *J. Phys. Chem.* **1960**, *64*, 1292.

[6] E. G. Shafrin, W. A. Zisman, *J. Phys. Chem.* **1960**, *64*, 519.

[7] B. E. Smart in *Chemistry of Organic Fluorine Compounds* (Eds. M. Hudlicky, A. E. Pavlath) ACS, Washington, **1995**, Chapter 3.

[8] E. Kissa in *Handbook of Fibre Science and Technology* (Eds. M. Lewin, S. B. Sello) Marcel and Dekker Inc., New York, **1984**, Chapter 2.

[9] E. F. Hare, E. G. Shafrin, W. A. Zisman, *J. Phys. Chem.* **1954**, *58*, 236.

[10] T. Shimizu in *Modern Fluoropolymers* (Ed. J. Scheirs) John Wiley & Sons Ltd., **1997**, Chapter 26.

[11] I. J. Park, S. B. Lee, C. K. Choi, K. J. Kim, *J. Colloid Interface Sci.* **1996**, *181*, 284.

[12] T. M. Chapman, R. Benrashid, K. G. Marra, J. P. Keener, *Macromolecules* **1995**, *28*, 331.

[13] J. Hopken, M. Moller, *Macromolecules* **1992**, *25*, 2482.

[14] R. R. Thomas, D. R. Anton, W. F. Graham, M. J. Darmon, B. B. Sauer, K. M. Stika, D. G. Swartzfager, *Macromolecules* **1997**, *30*, 2883.

[15] D. L. Schmidt, C. E. Coburn, B. M. DeKoren, G. E. Potter, G. F. Meyers, D. A. Fischer, *Nature* **1994**, *368*, 39.

[16] H. W. Fox, W. A. Zisman, *J. Colloid Sci.* **1950**, *5*, 514.

[17] S. R. Coulson, S. Brewer, C. Willis, J. P. S. Badyal *GB Pat.* **1997**, Appl. No. 9712338.4.

[18] H. Yasuda *Plasma Polymerization* Academic Press, Orlando, **1985**.

[19] M. E. Ryan, A. M. Hynes, J. P. S. Badyal, *Chem. Mater.* **1996**, *8*, 37.

[20] S. Morita, S. Ikeda, S. Ishibashi, M. Ieda, T. Norimatsu, C. Tamanaka, *International Symposium on Plasma Chemistry* **1981**, *5*, 272.

[21] W. Chen, A. Y. Fadeev, C. Hsieh, D. Oner, J. Youngblood, T. J. McCarthy, *Langmuir* **1999**, *15*, 3395.

[22] D. G. Shaw, M. G. Langlois, *Society of Vacuum Coaters* **1995**, 417.

[23] S. Morita, K. Yoneda, S. Ikeda, S. Ishibashi, J. Tamano, Y. Yamada, S. Hattori, M. Ieda *International Symposium on Plasma Chemistry* **1981**, *5*, 259.

[24] C. D. Enrlich, J. A. Basford, *J. Vac. Sci. Technol., A* **1992**, *10*, 1.

[25] K. Nakajima, A. T. Bell, M. Shen, *J. Appl. Polym. Sci.* **1979**, *23*, 2627.

[26] J. C. Brice, *Rev. Mod. Phys.* **1985**, *57*, 105.

[27] D. Briggs, M. P. Seah, in *Practical and Surface Analysis by Auger and X-ray Photoelectron Spectroscopy* Wiley, Chichester, **1983**.

[28] ASTM E-42.14 STM / AFM subcommittee recommendation for analysing and reporting surface roughness.

[29] J. D. Andrade in *Surface and Interfacial Aspects of Biomedical Polymers* (Ed. J. D. Andrade) Pleunum Press, New York, **1985**, Vol 1, Chapter 7.

[30] K. L. Mittal, *Contact Angle, Wettability and Adhesion* VSP BV, Netherlands, **1993**.

[31] F. M. Fowkes, *Ind. Eng. Chem.* **1964**, *56*, 40.

[32] J. J. Jasper, *J. Phys. Chem. Ref. Data* **1972**, *1*, 841.

[33] E. N. Dalal, *Langmuir* **1987**, *3*, 1009.

[34] B. W. Cherry, in *Cambridge Solid State Series: Polymer Surfaces* Cambridge University Press, Cambridge, **1981**, 28.

[35] A. R. Balkenende, H. J. A. P. Van de Boogaard, N. P. Willard, *Langmuir* **1998,** *14*, 5907.

[36] D. H. Kaelble, *J. Adhesion* **1970,** *2*, 66.

[37] D. T. Clark, D. Shuttleworth, *J. Polym. Sci. Chem. Ed.* **1980**, *18*, 27.

[38] G. Beamson, D. Briggs, *High Resolution XPS of Organic Polymers. The Scienta ESCA300 Database* John Wiley and Sons, Chichester, **1992**.

[39] C. Collette, C. Bourgeois, C. Taupin, C. Quet, M. D. Tran, Analusis **1989**, 17, 64.

[40] P. Graham, M. Stone, A. Thorpe, N. Nevell, J. Tsibouklis, *J. Proceedings of PRA Fluorine in Coatings III*, **1999**, 7.

[41] D. Lin-Vien, N. B. Colthup, W. G. Fateley, J. G. Grasselli, *The Handbook of Infrared and Raman Characteristic Frequencies of Organic Molecules* Academic Press, San Diego, **1991**.

[42] 3M water repellency test II water/alcohol drop test, 3M Test Methods (**Oct 1988**). 3M oil repellency test I, 3M Test Methods (Oct **1988**).

[43] V. Panchalingam, X. Chen, H. Huo, C. R. Savage, R. B. Timmons, R. C. Eberhart, *ASAIO Journal*, **1993**, 39, M305.

[44] H. Yasuda, T. Hsu, *J. Polym. Sci. Polym. Chem. Ed.* **1977**, *15*, 81.

[45] X. Chen, K. Rajeshwar, R. B. Timmons, J. J. Chen, M. R. Chyan, *Chem. Mater.* **1996**, *8*, 1067.

[46] A. G. Pittman, D. L. Sharp, B. A. Ludwig, *J. Polym. Sci. A-1* **1968**, *6*, 1729.

[47] R. Ramharack, T. H. Nguyen, *Journal of Polymer Science* **1987**, *25*, 93.

[48] R. E. Johnson, R. H. Dettre, Polym. Prep. *Am. Chem Soc. Div. Polym. Chem.* **1987**, *28*, 48.

[49] A. B. D. Cassie, S. Baxter, *Trans. Farad. Soc.* **1994**, *40*, 546.

[50] A. Hozumi, O. Takai, *Thin Solid Films* **1997**, *303*, 222.

[51] B. D. Washo, *Org. Coat. Appl. Polym. Sci. Proc.* **1982**, *47*, 69.

[52] P. Groning, A. Schneuwly, L. Schalapbach, M. T. Gale, *J. Vac. Sci. Technol.*, A **1996**, *14*, 3043.

[53] D. Sato, M. Jikei, M. kakimoto, *Polym. Prep. Am. Chem. Soc. Div. Polym. Chem.* **1998**, *39*, 926.

[54] F. Garbassi, M. Morra, E. Occhiello, *Polymer Surfaces: From Physics to Technology,* John Wiley and Sons, Chichester, **1994**.

[55] R. N. Wenzel, *Ind. Eng. Chem.* **1936**, *28*, 988.

[56] O. Takai, A. Hozumi, Y. Inoue, T. Komori, *Bull Mater Sci.* **1997**, *20*, 817.

[57] R. N. Wenzel, *J. Phys. Chem.* **1949**, *53*, 1466.

[58] J. L. Moillet, *Water Proofing and Water Repellency* Elsevier, London, **1963**.

CHAPTER 3

PLASMACHEMICAL FUNCTIONALISATION OF SOLID SURFACES WITH LOW SURFACE ENERGY PERFLUOROCARBON CHAINS

3.1. INTRODUCTION

Low surface energy finishes are important for many everyday applications [1], [2], [3], [4], e.g. protective coatings, biocompatible layers and stain resistant textiles. Conventionally, these have been made using solution phase polymerisation methods and applied by solvent casting techniques [5]. Here we describe an approach based upon plasma polymerisation, which offers a number of benefits: control of film thickness and composition regardless of substrate geometry [6], good adhesion to the underlying substrate geometry, minimal energy consumption, and negligible waste.

Plasma polymerisation comprises electromagnetic excitation of a precursor monomer vapour to produce ions (both positive and negative), neutrals, secondary electrons, and photons. Under favourable conditions, this can lead to coating deposition. Recently it has been demonstrated that highly specific polymerisation mechanisms can be investigated by modulating the electrical discharge [7], [8]. Therefore, since long terminal perfluoroalkyl chains are renowned for their liquid-repellency (oleophobicity as well as hydrophobicity [9]), pulsed plasma deposition of perfluorinated alkenes of the type $C_nF_{2n+1}CH=CH_2$, (a typical example being 1H,1H,2H-perfluoro-1-dodecene ($C_{10}F_{21}CH=CH_2$)) is reported. The deposited fluorocarbon films have been characterised using X-ray photoelectron spectroscopy (XPS), infrared spectroscopy, atomic force microscopy (AFM) and surface energy measurements. The comparison between deposition rates and functional group retention is also made for $C_{10}F_{21}CH=CH_2$ and its saturated analogue $C_{10}F_{21}CH_2$-CH_3.

3.2. EXPERIMENTAL

Experimental procedures were the same as reported in Chapter 2. The fluoromonomers used, 1H,1H,2H-perfluoro-1-dodecene and (perfluoro-n-decyl) ethane, were both obtained from Fluorochem and were 97% pure.

3.3. RESULTS

3.3.1. (a) 1H,1H,2H-perfluoro-1-dodecene ($C_{10}F_{21}CH=CH_2$)

The C(1s) XPS envelope for each deposited plasma polymer coating was fitted to six Gaussian Mg $K\alpha_{1,2}$ components [10] with equal full-widths-at-half-maximum (FWHM) [11]: $\underline{C}_xH_y$ at 285.0 eV, $\underline{C}$-CF_n at 286.6 eV, $\underline{C}F_n$ at 287.8 eV, $\underline{C}$F-CF_n at 289.3 eV, $\underline{C}F_2$ at 291.2 eV, and $\underline{C}F_3$ at 293.3 eV, Figure 3.1. Additional Mg $K\alpha_{3,4}$ X-ray satellite peaks shifted by ~9 eV towards lower binding energy [12] also needed to be taken into consideration. Continuous wave (CW) plasma polymerisation experiments indicated the rising perfluoroalkyl tail incorporation (i.e. the relative proportion of -$\underline{C}F_2$- groups)

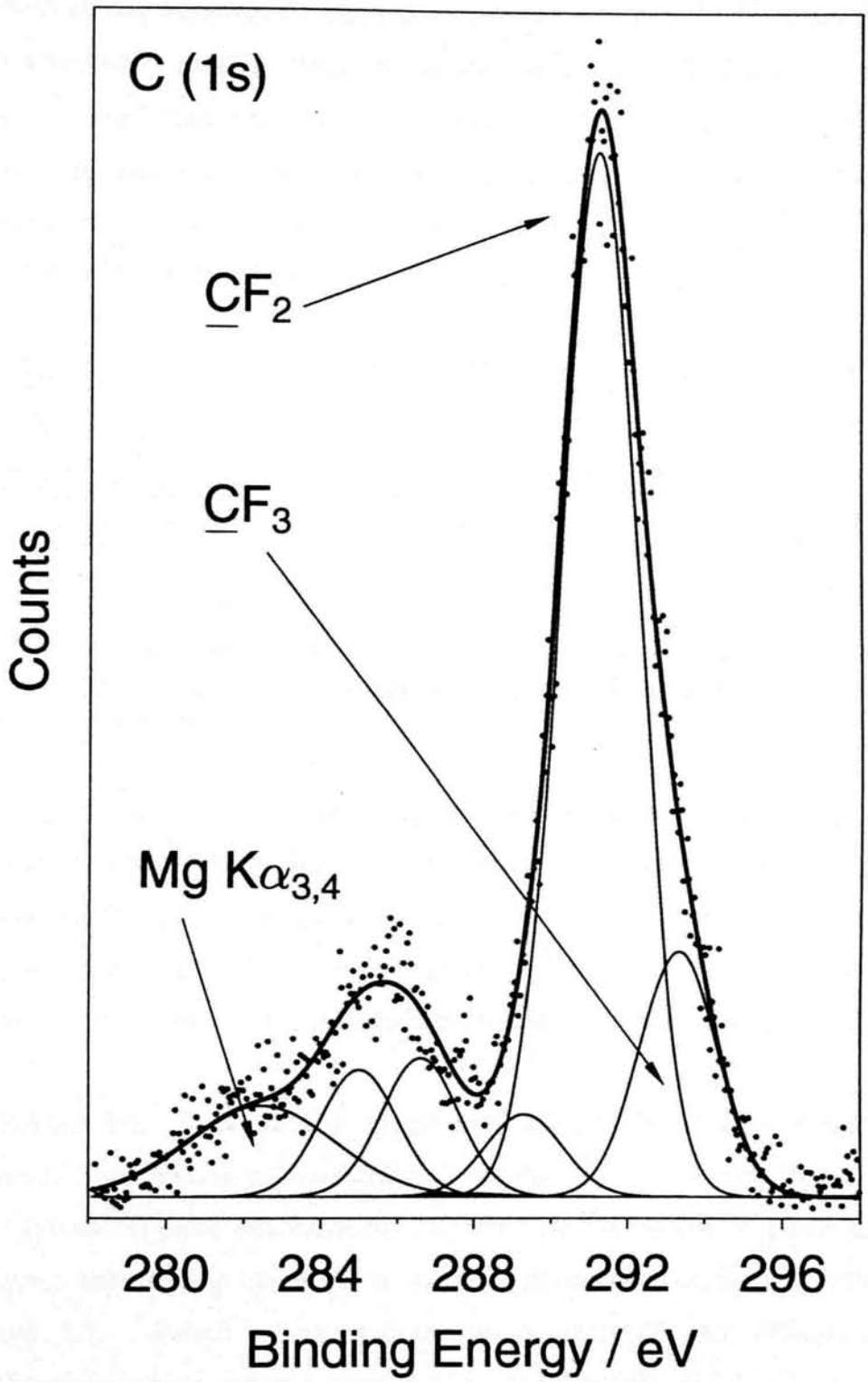

Figure 3.1 XPS C(1s) envelope for pulsed plasma polymerisation of 1H,1H,2H-perfluoro-1-dodecene at t_{on} = 20 μs, t_{off} = 20,000 μs, and P_p = 70 W.

with decreasing electrical discharge power, Figure 3.2. Even better structural retention was achieved by pulsing the system on the ms-μs timescale, Figures 3.3a, 3.3b and 3.3c. The optimum conditions were found to be P_p = 70 W, t_{on} = 20 μs and t_{off} = 20,000 μs, which is equivalent to an average power, <*P*>, of 0.07 W. A good correlation was found between the elemental composition of these films and the structure of the 1H,1H,2H-perfluoro-1-dodecene monomer unit, Table 3.1.

Treatment	Average Power (<P>)	F:C Ratio	%$\underline{C}F_2$	%$\underline{C}F_3$
Theoretical	-	1.75	75.0	8.3
Optimum Pulsed	0.07 W	1.56 ± 0.07	59.1 ± 3.7	16.6 ± 1.4
Continuous Wave	5 W	1.31 ± 0.07	28.0 ± 7.0	12.5 ± 11.3

Table 3.1 Compilation of the theoretical (corresponding to the monomer structure, CH_2=$CHC_{10}F_{21}$), and actual chemical environments measured by XPS for 1H,1H,2H-perfluoro-1-dodecene.

The higher than predicted concentration of $\underline{C}F_3$ functionalities in the C(1s) envelope for the pulsed plasma polymer layer can be attributed to the surface sensitivity of the XPS technique, detecting the alignment of perfluoroalkyl chains away from the surface to give a greater signal from the CF_3 group. Similar behaviour has been observed previously for solution phase polymerised perfluoroalkyl monomers [13].

Preferential loss of the following characteristic alkene infrared absorption features was observed upon plasma polymerisation of 1H,1H,2H-perfluoro-1-dodecene [14]: 1424 cm^{-1} (alkene in-plane deformation), 710-1067 cm^{-1} (CH_2 out of plane deformation, wagging and twisting vibrations as well as CH in- and out-of-plane deformations), Figure 3.4. Pulsed plasma polymerisation produced less broadening of the perfluoroalkyl chain absorption bands [14] at 1120-1280 cm^{-1} (CF_2) and 1120-1350 cm^{-1} (CF_3). This is consistent with greater structural retention compared to continuous wave conditions (i.e. less rearrangement, fragmentation and crosslinking reactions).

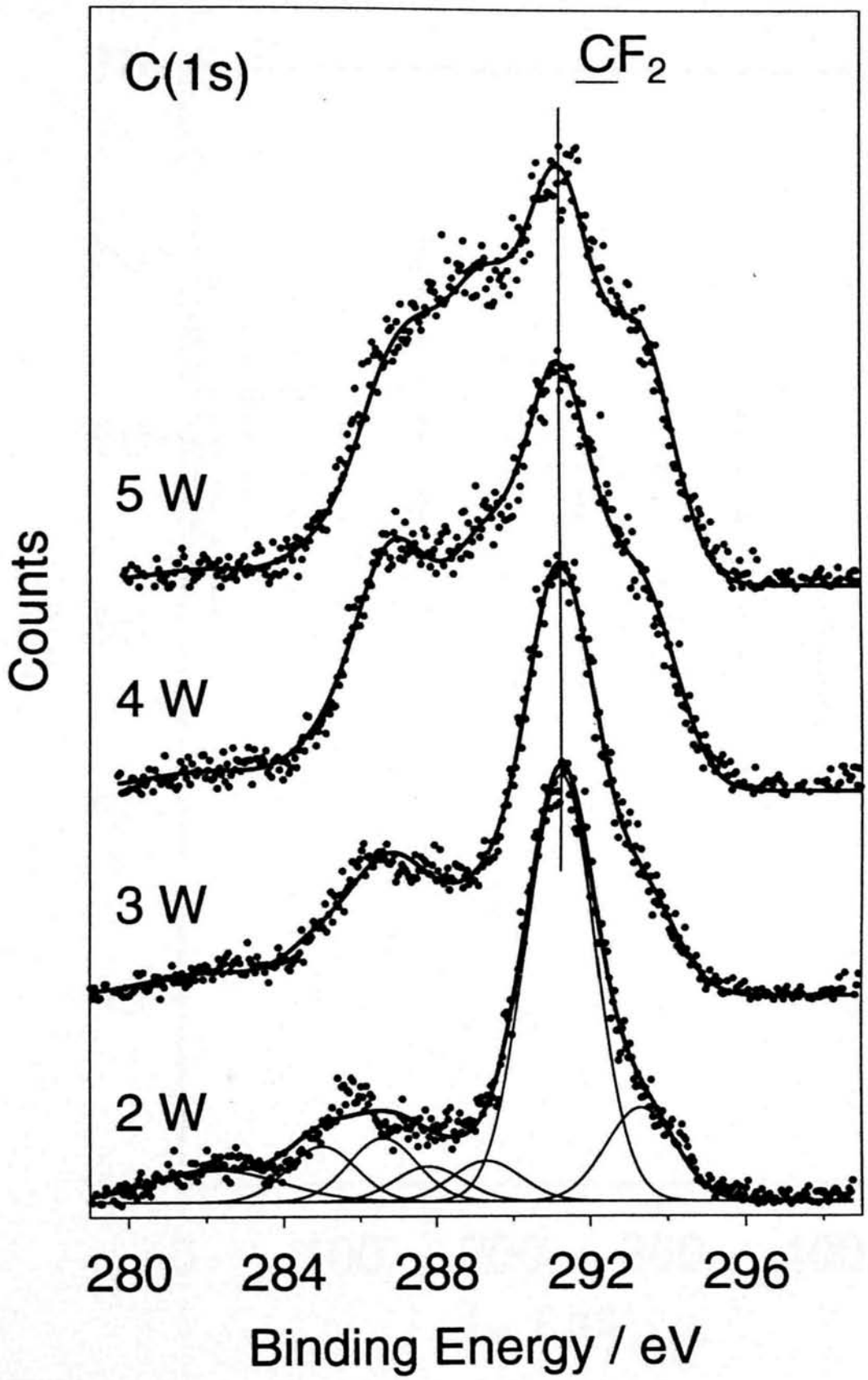

Figure 3.2 XPS C(1s) spectra of continuous wave plasma polymerisation of 1H,1H,2H-perfluoro-1-dodecene at various powers.

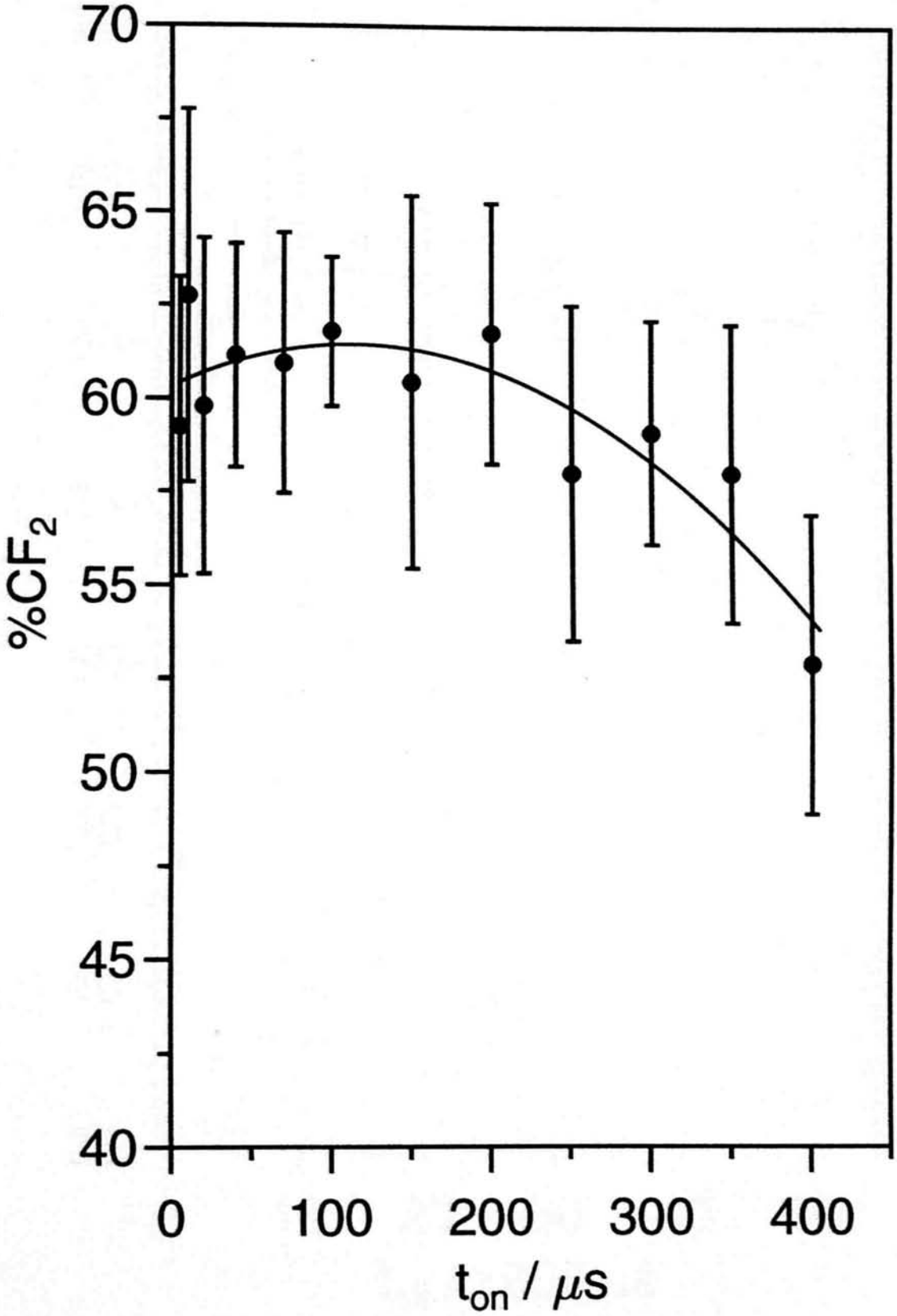

Figure 3.3a Plot of CF_2 group incorporation as a function of t_{on} (at fixed t_{off} = 20,00 μs and P_p = 70 W).

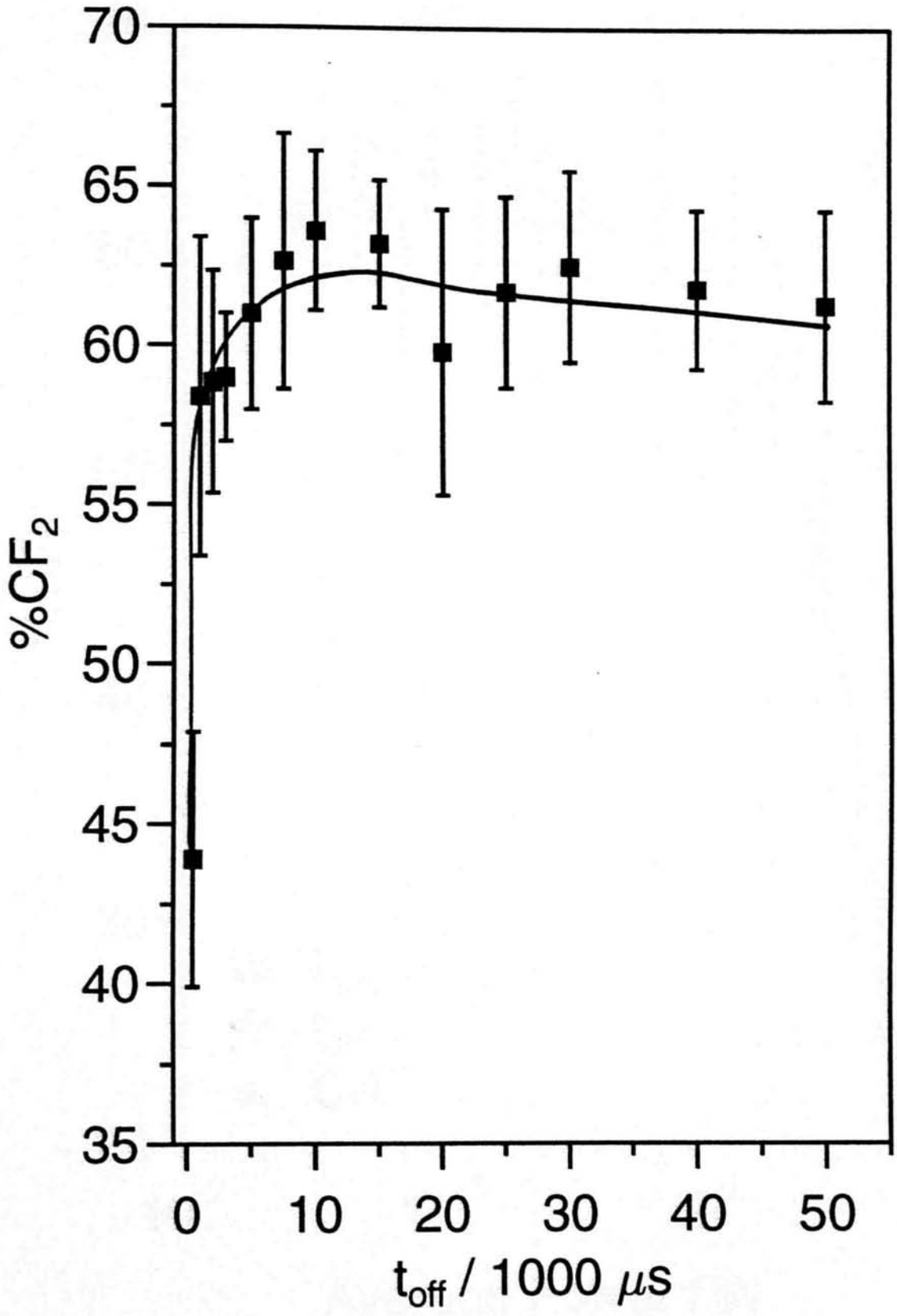

Figure 3.3b Plot of CF_2 group incorporation as a function of t_{off} (at fixed t_{on} = 20 μ and P_p = 70 W).

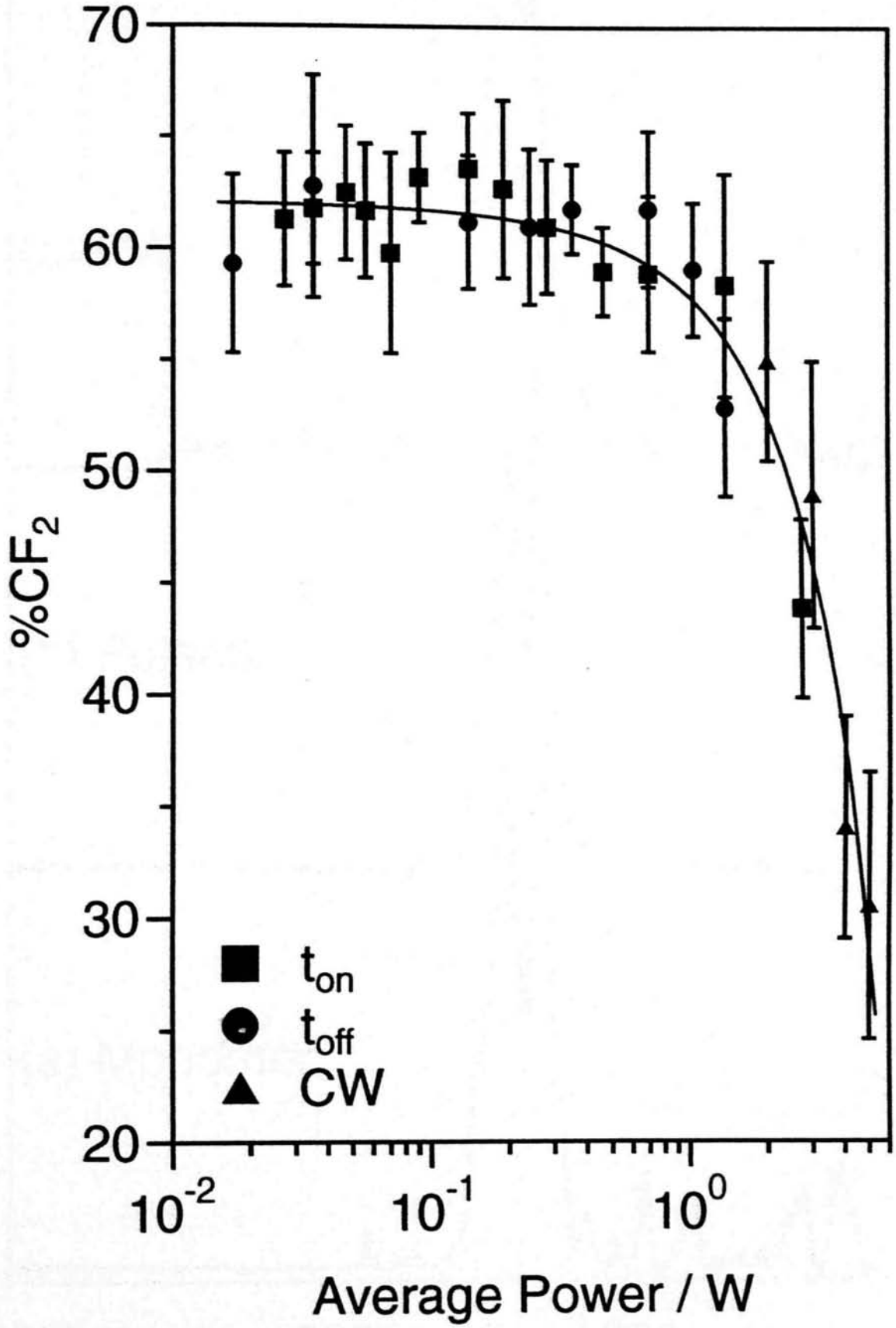

Figure 3.3c Plot of CF_2 group incorporation as a function of average power.

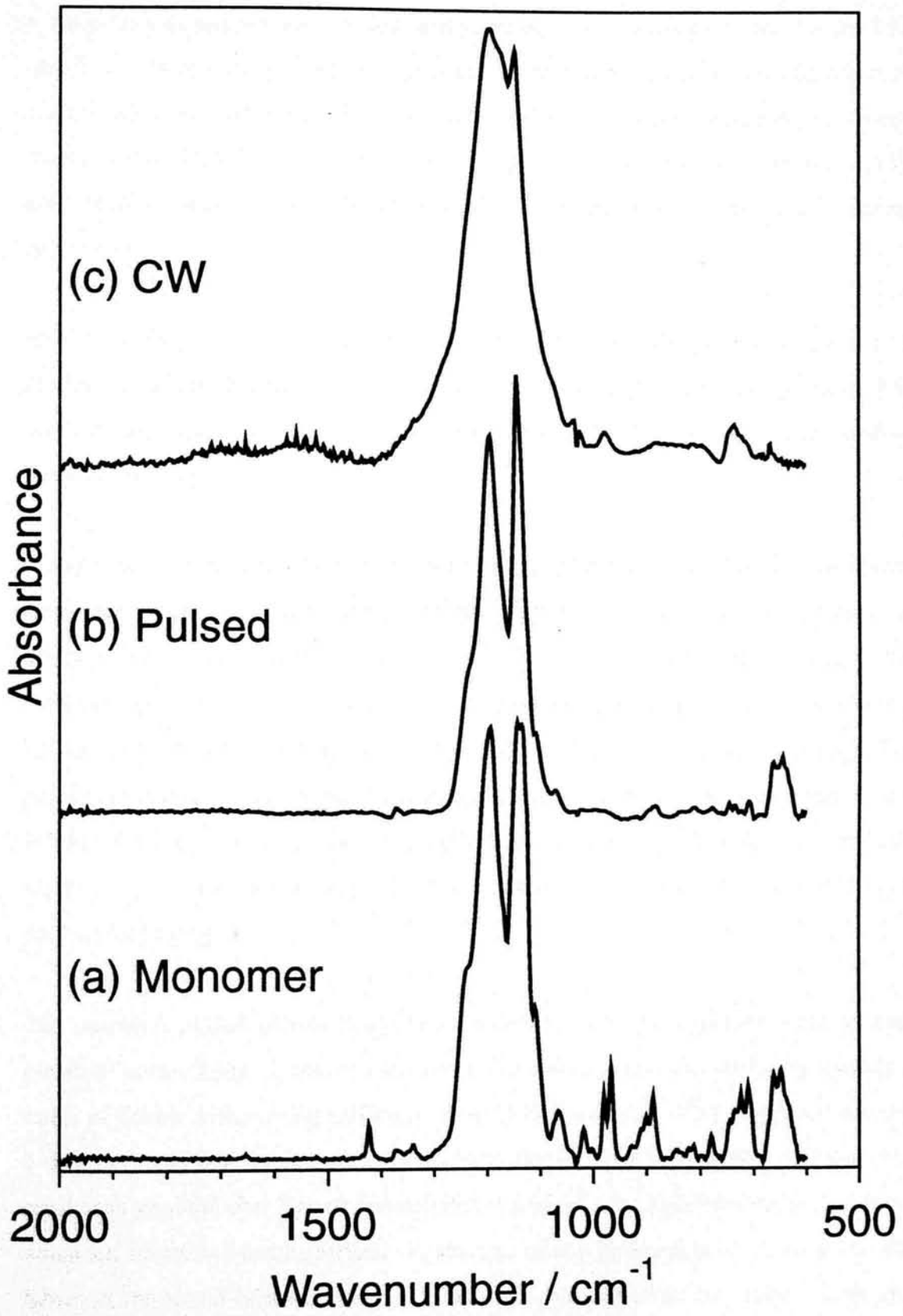

Figure 3.4 Infrared spectra of: (a) 1H,1H,2H-perfluoro-1-dodecene monomer; (b) optimum pulsed plasma polymerisation conditions (t_{on} = 20 μs, t_{off} = 20,000 μs, and P_p = 70 W); and (c) 5 W continuous wave.

A maximum deposition rate was attained at close to 1 W average power, Figure 3.5a and 3.5b. In this range, greater deposition is observed during pulsed compared to continuous wave conditions. The most likely explanation for this being that the plasma sheath potential and VUV flux are significantly lower during pulsing conditions [15], and therefore ion-assisted ablation and VUV damage will be less likely during deposition.

AFM analysis gave RMS roughness values of 0.7 nm for the flat glass substrate and 11 nm for the 1H,1H,2H-perfluoro-1-dodecene pulsed plasma polymer coating, Figure 3.6. Surface roughness on the sub-micron scale was clearly discernible in the corresponding AFM phase image.

Water contact angle measurements taken on plasma polymer coated flat glass substrates confirmed there is a correlation between liquid repellency and the extent of perfluoroalkyl chain retention, Figure 3.7. For optimum structural retention, the combined geometric mean-Young's equation gave surface energy values as low as $\gamma = 8.3$ mN m^{-1} (where $\gamma_s^d = 8.2$ mN m^{-1} and $\gamma_s^p = 0.1$ mN m^{-1}). The presence of negligible polar contribution to the total surface energy under these conditions meant that it was valid to use a homologous series of alkane probe liquids to make a Zisman plot; this yielded $\gamma_c = 1.5$ mN m^{-1}, Figure 3.8. This is significantly lower than for PTFE ($\gamma_c = 18.5$ mN m^{-1}) [16].

The optimum pulsed plasma deposition conditions were subsequently used to coat pieces of cotton fabric in order to test for hydrophobicity and oleophobicity towards a range of liquids with varying surface tensions [17], Chapter 2. This comprised placing 3 drops of each test liquid onto coated cotton fabric. The surface was considered to repel each liquid if after 30 s (for oleophobicity and 10 s for hydrophobicity), the drops remained spherical / hemispherical, i.e. absence of any penetration or wicking into the fabric at the liquid-fabric interface. Repellency was observed for water / isopropyl alcohol (IPA) mixtures of up to 90% IPA (hydrophobicity), and also alkane chains as short as dodecane (oleophobicity), Figure 3.9.

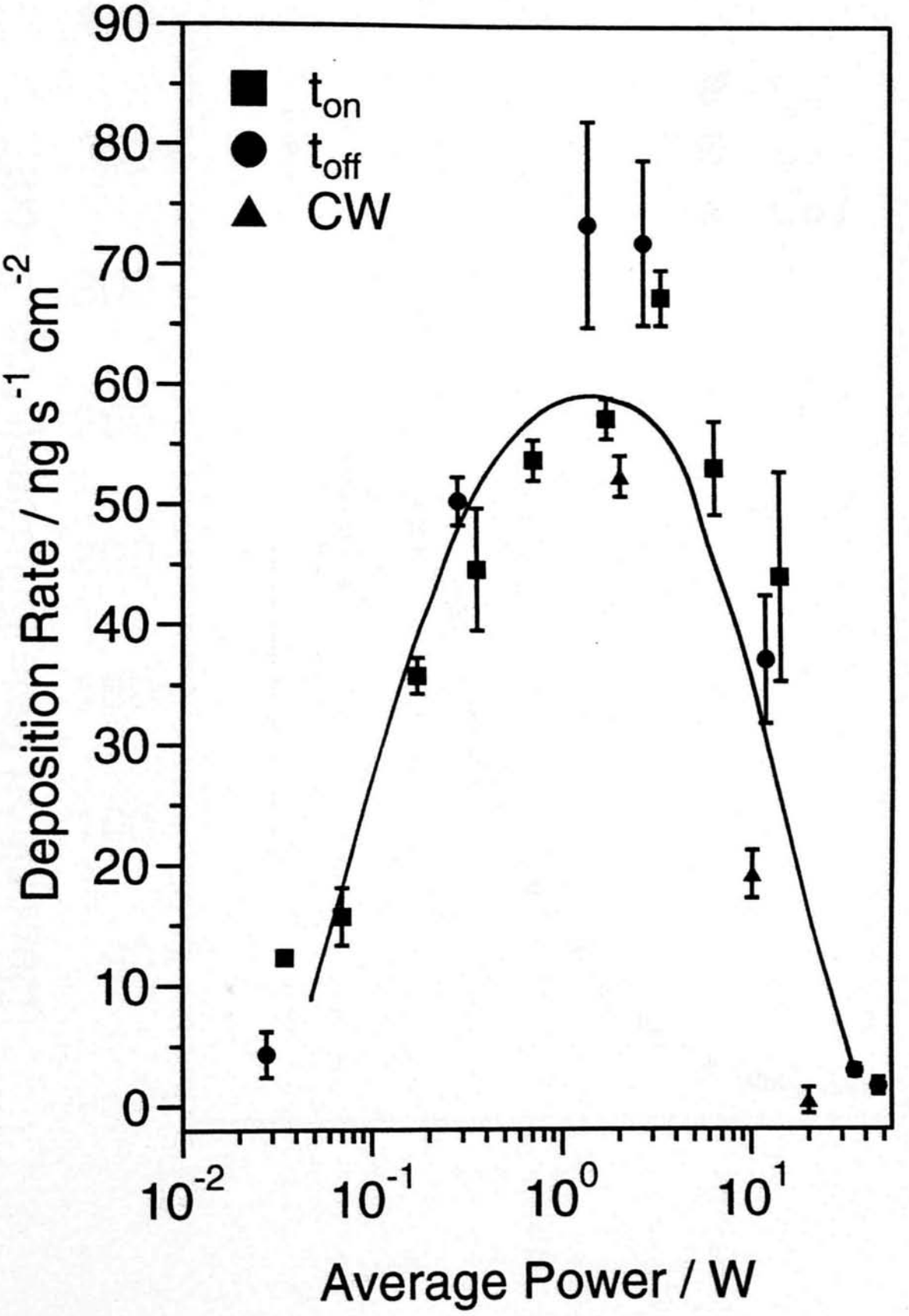

Figure 3.5a Deposition rate studies for 1H,1H,2H-perfluoro-1-dodecene.

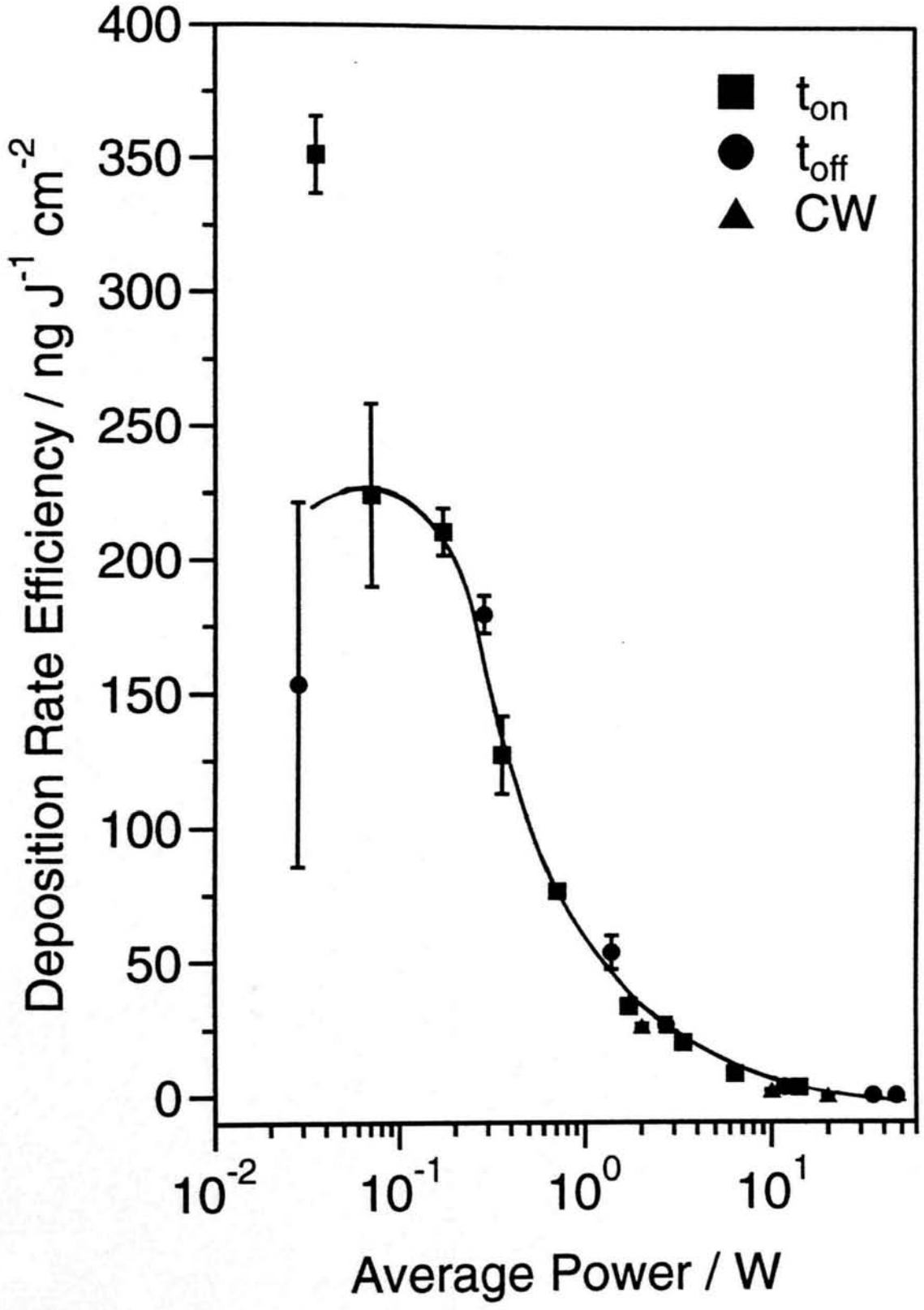

Figure 3.5b Deposition rate efficiency studies for 1H,1H,2H-perfluoro-1-dodecene.

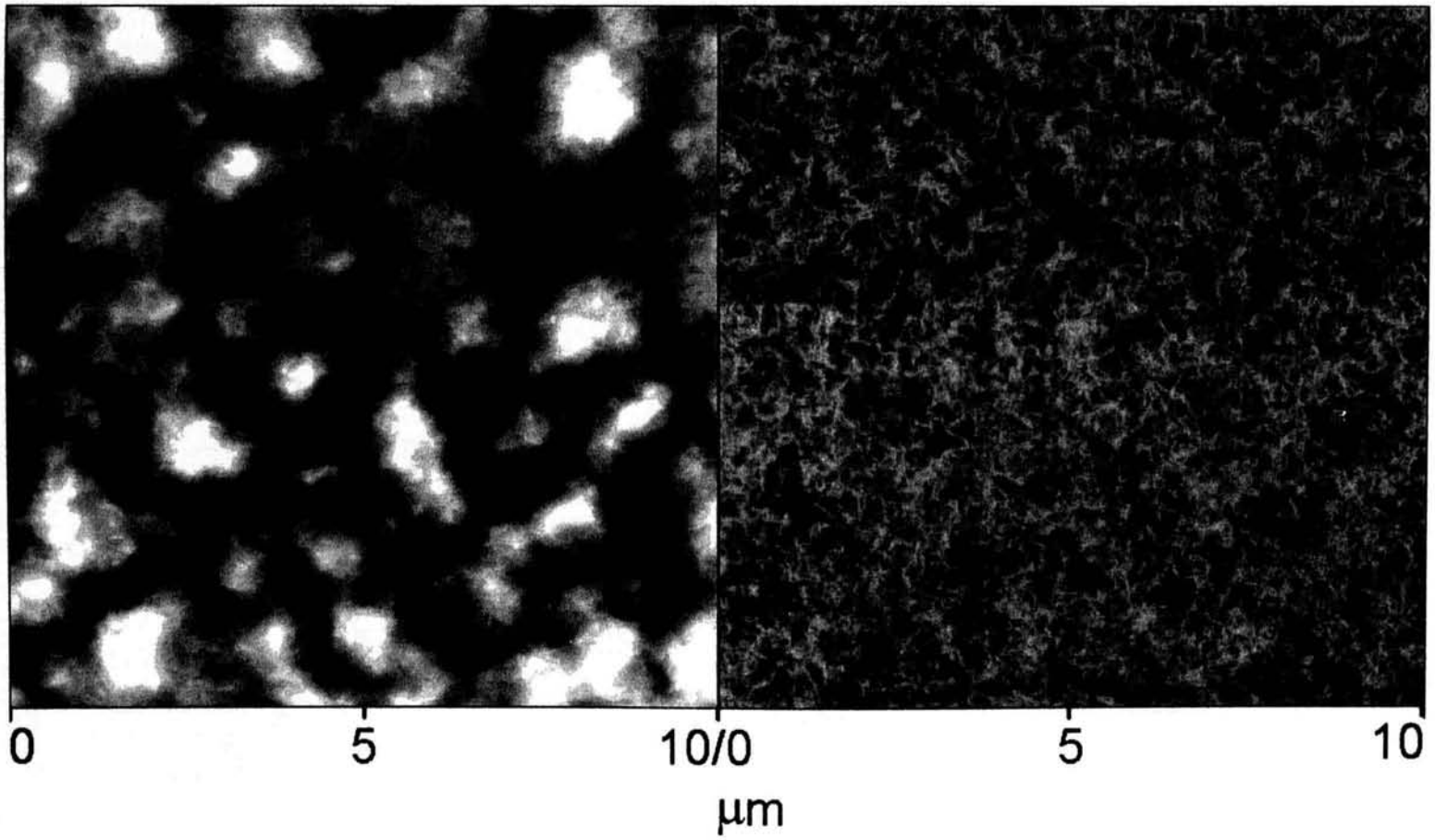

Figure 3.6 AFM micrographs of pulsed plasma polymer of 1H,1H,2H-perfluoro-1-dodecene (t_{on} = 20 µs, t_{off} = 20,000 µs and P_P = 70 W): height image shown on LHS (z = 100 nm) and corresponding phase image on RHS.

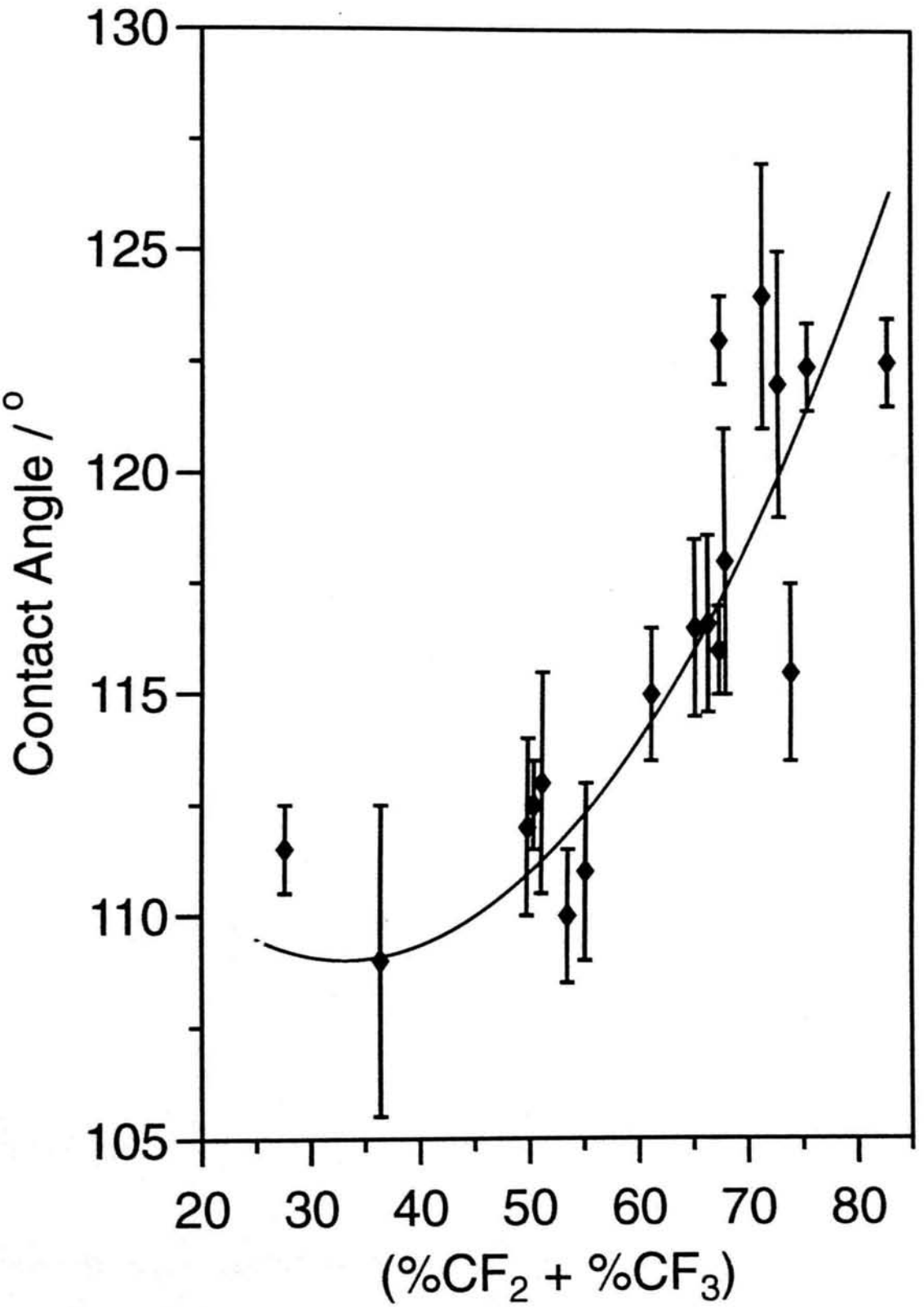

Figure 3.7 Water contact angle versus (%CF_2 + %CF_3) concentration in the plasma polymer films using the sessile drop technique.

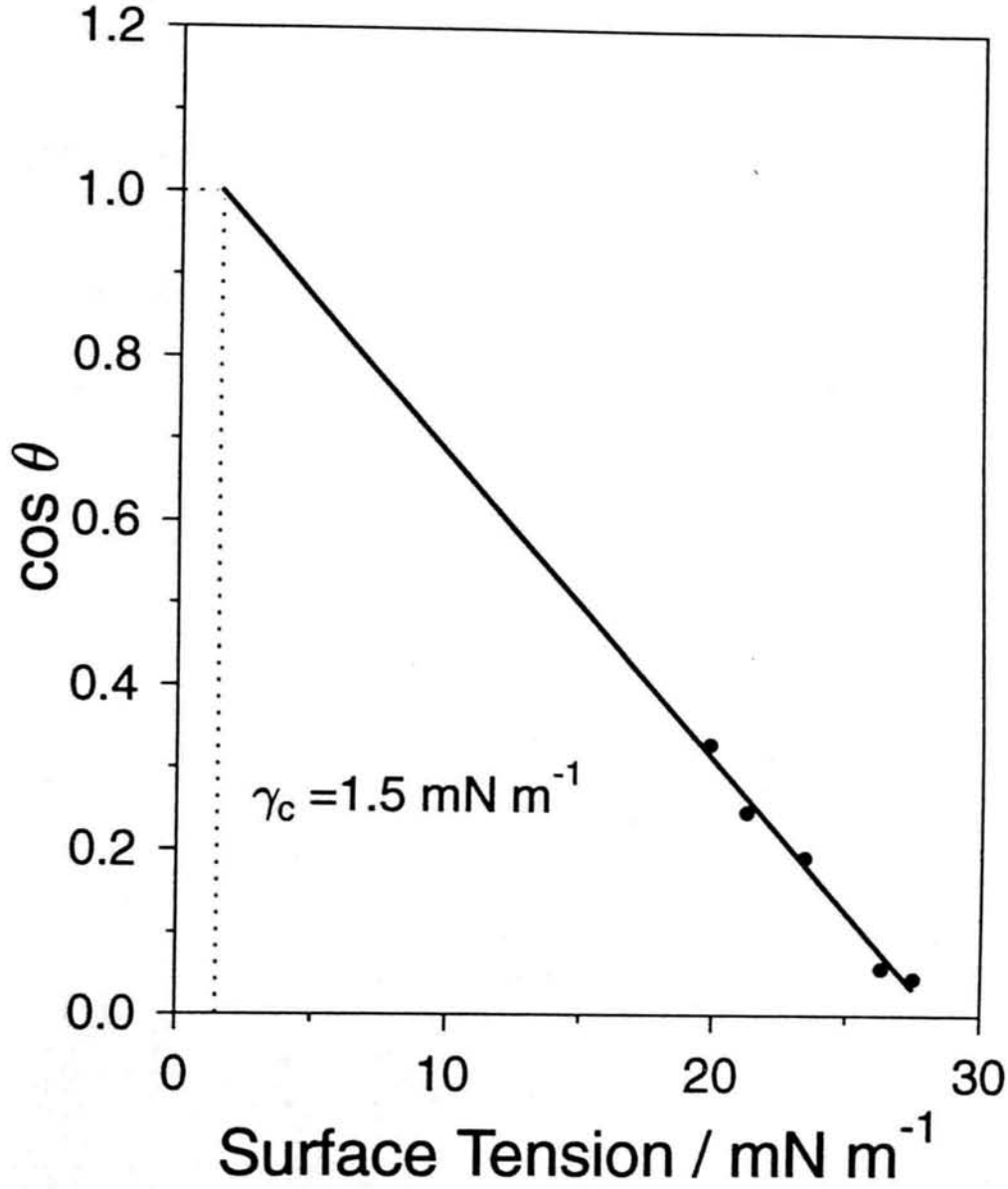

Figure 3.8 Zisman plot of pulsed plasma polymer coated glass slide (t_{on} = 20 μs, t_{off} = 20,000 μs, P_p = 70 W).

3.3.2. (b) Role of the Polymerisable End-Group

The pulsed plasma polymerisation of 1H,1H,2H-perfluoro-1-dodecene ($C_{10}F_{21}CH{=}CH_2$) was compared with its saturated analogue (perfluoro-n-decyl) ethane ($C_{10}F_{21}CH_2\text{-}CH_3$) as a function of pulse frequency at a fixed duty cycle and peak power. XPS showed that greater structural retention of the perfluoroalkyl chain for the alkene monomer, and this improves at shorter on-times, Figure 3.10 (R_f = $C_{10}F_{21}$). A comparison of deposition rates at the duty cycle pulse frequency corresponding to the

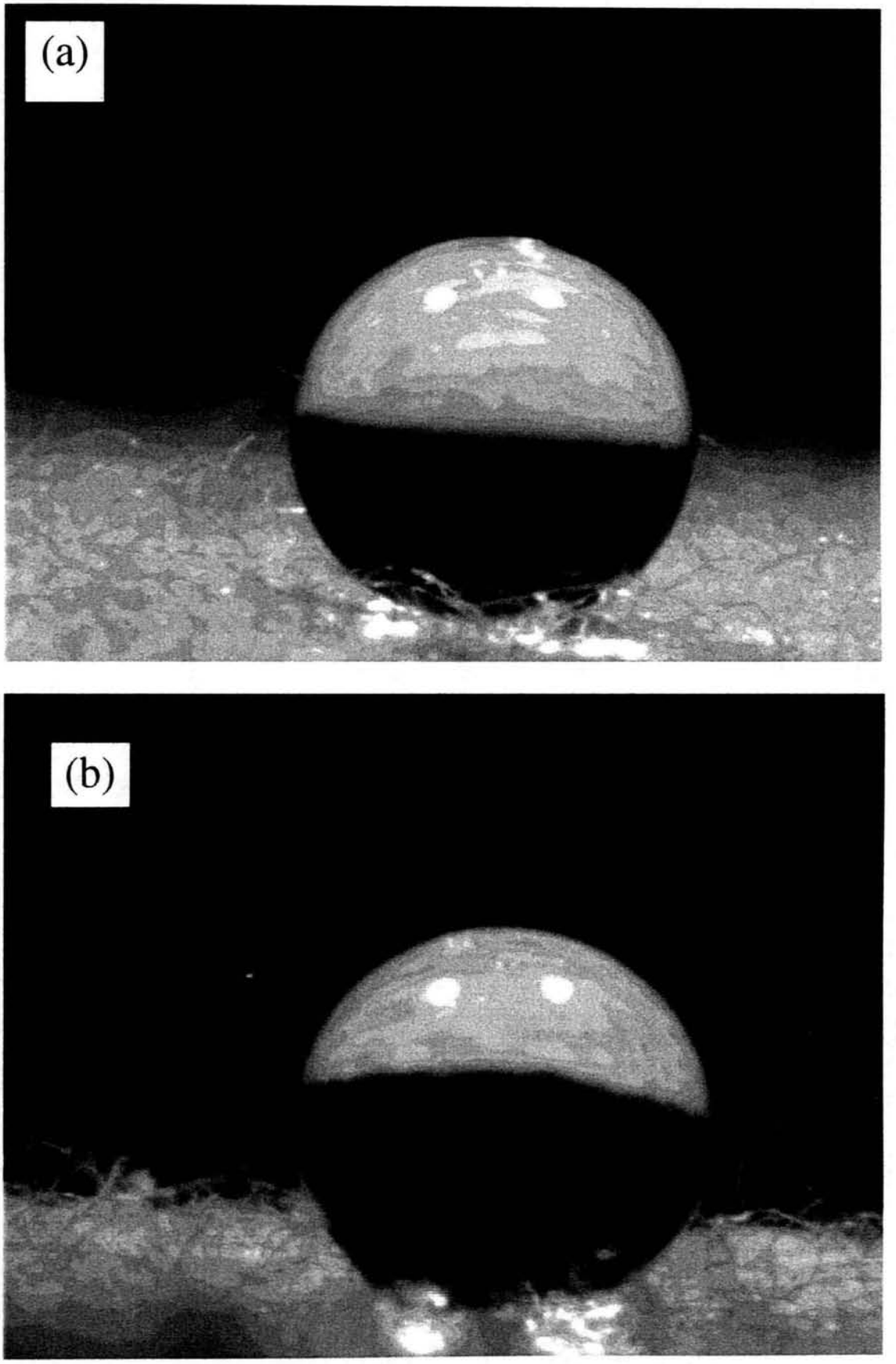

Figure 3.9 Optical images illustrating liquid repellency (2 µl droplet volume) for 1H,1H,2H-perfluoro-1-dodecene pulsed plasma polymer layer deposited onto cotton fabric (t_{on} = 20 µs, t_{off} = 20,000 µs, P_p = 70 W): (a) pure water droplet; and (b) dodecane droplet.

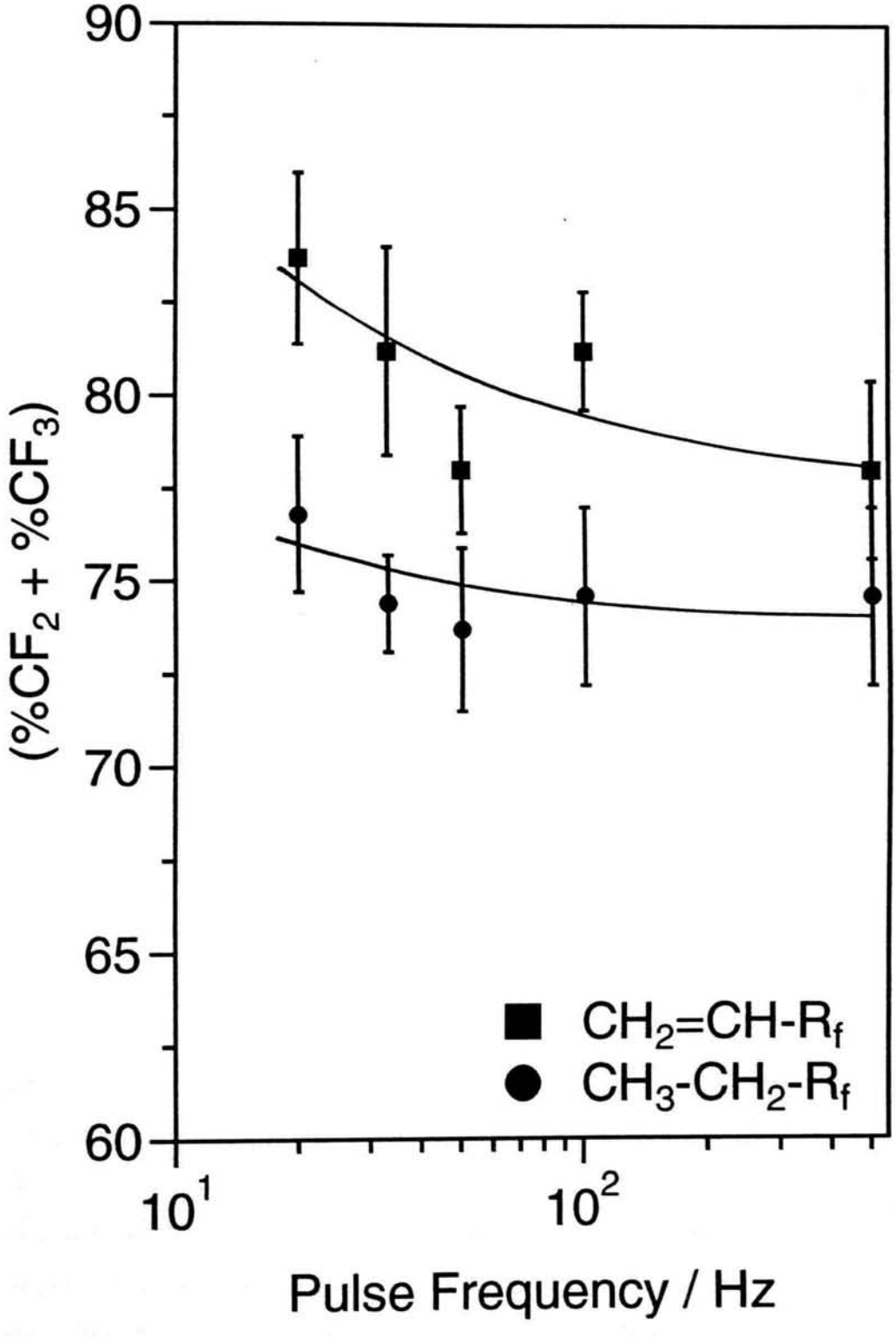

Figure 3.10 Comparison of pulsed plasma polymerisation of 1H,1H,2H-perfluoro-1-dodecene versus (perfluoro-n-decyl) ethane: as a function of pulse frequency ($1/(t_{on}+t_{off})$), where average power = 0.07 W and P_P = 70 W) and (%CF_2 + %CF_3) group retention.

optimum conditions showed that the alkene is more amenable to pulsed plasma polymerisation, Table 3.2.

Monomer	Deposition rate / ng s^{-1} cm^{-2}
1H,1H,2H-perfluoro-1-dodecene	15.7 ± 2.4
(Perfluoro-n-decyl) ethane	8.4 ± 0.4

Table 3.2 Comparison of deposition rates (t_{on} = 20 μs, t_{off} = 20,000 μs, and P_p = 70 W).

3.4. DISCUSSION

The greater incorporation of >$\underline{C}F_2$ groups observed during electrically pulsed plasma polymerisation compared to continuous wave conditions is consistent with less fragmentation and damage of the perfluoroalkyl tail belonging to the monomer, Table 3.1. Lower average powers produces a drop in plasma sheath potential, leading to milder ion bombardment of the growing film [15], and less VUV irradiation [18]; both of these effects will help to minimise surface damage during the plasma on-period. The low deposition rate observed at very short duty cycles can be attributed to insufficient monomer activation to effectively sustain polymerisation under these conditions. Intermediate pulse duty cycles approach a maximum corresponding to the highest ratio of polymerisable species to non-polymerisable / ablative species in the plasma.

Eventually the deposition rate falls towards continuous wave conditions, as a consequence of more energetic species making ablation a competing process. In order to factor out the dependence on average power, the deposition rate efficiency was considered (defined as deposition rate divided by average power) [19], Figure 3.5b. It is found that the deposition rate per joule of energy goes up with decreasing average power. This can be taken as being indicative of the active sites generated during the on-period (via VUV irradiation, ion or electron bombardment etc.) polymerising via conventional free radical pathways. This can occur either in the gas phase or at the plasma-substrate interface. The greater structural retention and deposition rate observed for 1H,1H,2H-perfluoro-1-dodecene compared to (perfluoro-n-decyl) ethane is consistent with conventional polymerisation taking place at the double bond during

the off-period. Compared to conventional solvent-based liquid-repellent coatings, the described plasma polymerisation method benefits from not requiring additional non-fluorochemical reagents (e.g. catalysts, crosslinking agents, etc) [20]. Overall this should produce a cleaner fluoropolymer material, which will contribute towards an improvement in liquid repellency. This is reflected in the low critical surface tension value, γ_c = 1.5 mN m^{-1} measured for the pulsed plasma polymer. Any distortion in the calculated critical surface tension value, γ_c, to an abnormally low value as a consequence of surface roughness is unlikely; since the series of alkane probe liquids all exhibit contact angles less than 90°. This means that Wenzels law [21] would have predicted

lower liquid contact angles compared to the true values (roughness decreases the contact

angle for liquids exhibiting contact angles less than 90° on flat surfaces). Therefore $cos\theta$ will be greater for each probe liquid on the Zisman plot, leading to an increase in γ_c. Porosity in the film leading to a composite interface containing trapped air can also be ruled out due to the absence of low contact angle hysteresis normally associated with a composite interface [22], [23] (advancing and receding contact angle values, θ_{adv} / θ_{rec} = 127° / 86° and 74 °/ 35° for water and octane respectively).

3.5. CONCLUSIONS

Pulsed plasma polymerisation of 1H,1H,2H-perfluoro-1-dodecene produces a low surface energy coating containing long perfluoroalkyl chains. Comparison with its saturated analogue, (perfluoro-n-decyl) ethane shows that the alkene bond significantly improves structural retention and deposition rate by facilitating conventional polymerisation reaction pathways during the off-period.

3.6. REFERENCES

[1] B. Boutevin, Y. Pietrasanta in *Les Acrylates et Polyacrylates Fluorés: Dérivés et Applications* EREC, Paris, **1988**.

[2] L. Klinger, J. R. Griffith, *Org. Coat. Appl. Polym. Sci.* **1983**, *48*, 407.

[3] C. Bonardi, *Eur. Patent Appl.* EP 426,530, Elf Atochem, inv. **08.05.91**.

[4] C. G. DeMarco, A. J. Macquade, S. J. Kennedy, *Mod. Text. Mag.* **1960**, *2*, 50.

[5] I. J. Park, S. B. Lee, C. K. Choi, K. J. Kim, *J. Colloid Interface Sci.* **1996**, *181*, 284.

[6] C. M. Chan, T. M. Ko, H. Hiraoka, *Surf. Sci. Rep.* **1996**, *24*, 1.

[7] C. R. Savage, R. B. Timmons, *Chem. Mater.* **1991**, *3*, 575.

[8] M. E. Ryan, A. M. Hynes, J. P. S. Badyal, *Chem. Mater.* **1996**, *8*, 37.

[9] E. Kissa in *Handbook of Fibre Science and Technology* (Eds. M. Lewin, S. B. Sello) Marcel and Dekker Inc., New York, **1984**, Chapter 2.

[10] G. Beamson, D. Briggs, *High Resolution XPS of Organic Polymers. The Scienta ESCA300 Database* John Wiley and Sons, Chichester, **1992**.

[11] J. F. Evans, J. H. Gibson, J. F. Moulder, J. S. Hammond, H. Goretzki, *Fresenius Z. Anal. Chemie*, **1984**, *319*, 841.

[12] D. Briggs, M. P. Seah, in *Practical and Surface Analysis by Auger and X-ray Photoelectron Spectroscopy* Wiley, Chichester, **1983**.

[13] S. R. Coulson, J. P. S. Badyal, C. R. Willis, S. A. Brewer, *Ultra Low Surface Energy Plasma Polymer Films*, in preparation.

[14] D. Lin-Vien, N. B. Colthup, W. G. Fateley, J. G. Grasselli, *The Handbook of Infrared and Raman Characteristic Frequencies of Organic Molecules* Academic Press, San Diego, **1991**.

[15] V. Panchalingam, X. Chen, H. Huo, C. R. Savage, R. B. Timmons, R. C. Eberhart, *ASAIO Journal*, **1993**, 39, M305.

[16] H. W. Fox, W. A. Zisman, *J. Colloid Sci.*, **1950**, *5*, 514.

[17] 3M water repellency test II water/alcohol drop test, 3M Test Methods 1st Oct 1988. 3M oil repellency test I, 3M Test Methods 1st Oct 1988.

[18] H. Yasuda, T. Hsu, *J. Polym. Sci. Polym. Chem. Ed.* **1977**, *15*, 81.

[19] X. Chen, K. Rajeshwar, R. B. Timmons, J. J. Chen, M. R. Chyan, *Chem. Mater.* **1996**, *8*, 1067.

[20] T. Shimizu in *Modern Fluoropolymers* (Ed. J. Scheirs) John Wiley & Sons Ltd., **1997**, Chapter 26.

[21] R. W. Wenzel, *Ind. Eng. Chem.* **1936**, *28*, 988.

[22] A. B. D. Cassie, S. Baxter, *Trans. Farad. Soc.* **1994**, *40*, 546.

[23] F. Garbassi, M. Morra, E. Occhiello, *Polymer Surfaces: From Physics to Technology* John Wiley and Sons, Chichester, **1994**.

CHAPTER 4

ROUGH SURFACES

4.1. INTRODUCTION

It is well known that repellency is dependent on both the chemistry and roughness of the solid surface [1], [2]. Chapter 2 addressed how to optimise the chemistry at the solid surface in order to maximise repellency on flat substrates. It has been the aim of this piece of work to optimise surface roughness and then to pulse plasma deposit the repellent coating used throughout Chapter 2 (1H,1H,2H,2H-heptadecafluorodecyl acrylate) to gain maximum repellency. The work discussed here is divided into three parts. Part A addresses the theory behind the effect surface roughness has on contact angle formation. Part B looks at roughening two different solid surfaces. Finally part C concentrates on the deposition of the fluorinated acrylate onto commercially available rough surfaces to try and ascertain the optimum rough geometry for maximum contact angle formation.

4.2. PART A

Roughening of a solid surface enhances its wettability properties [1]. This could lead to either an increase or decrease in contact angles, depending on the surface chemistry.

4.2.1. Theory

It has already been shown in Chapter 1 that the adhesion tension, τ, is given by Equation [3]:-

$$\tau = \gamma_{SV} - \gamma_{SL} \qquad 4.1$$

and Young's Equation [4],

$$\gamma_{SV} = \gamma_{SL} + \gamma_{LV}\cos\theta \qquad 4.2$$

Where γ_{SV}, γ_{SL}, and γ_{LV} are the surface energies of the solid-vapour, solid-liquid and the liquid-vapour interface respectively. If the surface was roughened microscopically and the roughness factor is denoted by r, then the adhesion tension on a rough surface (τ^R) becomes [3]:-

$$\tau^R = r(\gamma_{SV} - \gamma_{SL}) \qquad 4.3$$

since each surface area and therefore each surface component is multiplied by r. The apparent contact angle on the rough surface, ϕ, will be given by:-

$$\cos\phi = \frac{\tau^R}{\gamma_{LV}} \qquad 4.4$$

so $$\cos\phi = \frac{r(\gamma_{SV} - \gamma_{SL})}{\gamma_{LV}}$$

therefore $$\cos\phi = r\cos\theta$$

or $$\frac{\cos\phi}{\cos\theta} = r \qquad 4.5$$

Equation 4.5 is known as Wenzel's equation where r is the ratio of the area of the actual surface to that of the smooth surface. It shows that if the true (intrinsic)

contact angle of a liquid on a flat surface is greater than 90°, it will increase if the surface was roughened. Conversely for a surface with a contact angle less than 90°, roughening the surface will reduce the contact angle. This can be appreciated more fully by considering Cassie and Baxter's extension of Wenzel's theory [5], whereby a composite interface is considered, Figure 4.1. The rough surface is depicted as a series of adjacent crests and troughs and the original adhesion tension as shown in Equation 4.3 has been complicated further.

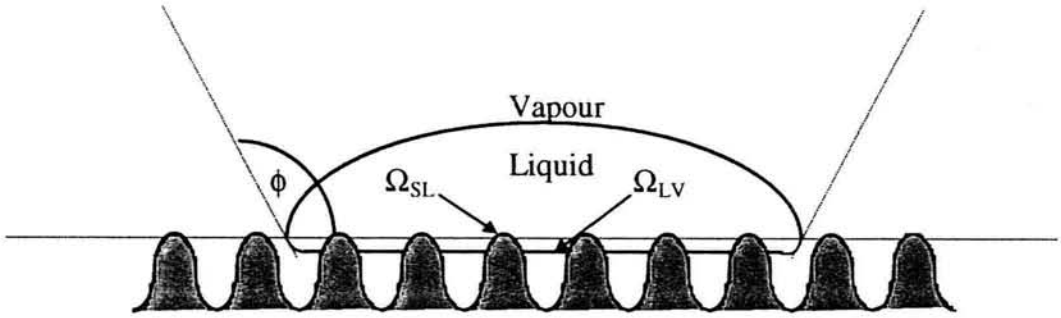

Figure 4.1 Schematic drawing of a liquid droplet sitting on a rough surface.

By considering the polymer-liquid interface to have an area of Ω_{SL} and the liquid-vapour interface to have an area of Ω_{LV}, the adhesion tension of a composite interface is given by Equation 4.6:-

$$\tau^R = \Omega_{SL}(\gamma_{SV} - \gamma_{SL}) - \Omega_{LV}\gamma_{LV} \qquad 4.6$$

The depth of the crevices in the surface does not alter the contact angle and hence no additional polymer-vapour interface term is present in Equation 4.6. Therefore the deciding factors for the surface roughness are the width of the asperities and the distance between them i.e. Ω_{SL} and Ω_{LV}. Now by substituting Equation 4.6 into Equation 4.4 gives:-

$$\cos\phi = \frac{\Omega_{SL}(\gamma_{SV} - \gamma_{SL})}{\gamma_{LV}} - \Omega_{LV} \qquad 4.7$$

and knowing

$$\cos\theta = \frac{\left(\gamma_{SV} - \gamma_{SL}\right)}{\gamma_{LV}}$$

(a rearrangement of Equation 4.2), then

$$\cos\phi = \Omega_{SL}\cos\theta - \Omega_{LV} \qquad 4.8$$

From Figure 4.1 it can be presumed that the wetting liquid is in contact with two different fractions of the surface, one of which is the substrate crest (ε_a) and the other being the medium in between the crests (ε_b). If θ_a and θ_b are the intrinsic contact angles of the liquid on each of the two mediums respectively, then the apparent contact angle is given by [6], [7]:-

$$\cos\phi = \varepsilon_a \cos\theta_a + \varepsilon_b \cos\theta_b \qquad 4.9$$

This equation has two possible simplifications depending on whether the roughened surface, ε_a, is hydrophobic or hydrophilic. In the former case, water can not enter the troughs and so the surface is said to comprise an air / surface composite. As the contact angle of water on air is 180°, Equation 4.9 is simplified by Equation 4.10 where ε is the fraction of air on the surface and θ is the contact angle of water on the original, flat substrate surface. When this occurs $\phi > \theta$.

$$\cos\phi = (1-\varepsilon)\cos\theta - \varepsilon \qquad 4.10$$

If, on the other hand, the surface is hydrophilic the water will freely enter the troughs; and with the contact angle of water on water being 0° Equation 4.9 becomes:-

$$\cos\phi = (1-\varepsilon)\cos\theta + \varepsilon \qquad 4.11$$

and $\phi < \theta$.

4.3. PART B

4.3.1. Ultra-Low Surface Energy from Modified PTFE

4.3.1.1. Introduction

Liquid repellency of solid surfaces is critical for many applications, these include the prevention of icing in cold weather [8], stopping clotting in artificial blood vessels [9], and stain resistant textiles [10]. In this context, PTFE is considered to be the "benchmark" low surface energy material, displaying water repellency [11] in combination with other desirable properties such as high thermal stability, chemical inertness and a low friction coefficient [12]. However, PTFE has limitations in that it exhibits poor repellency towards low surface tension liquids such as oils. One way to improve liquid repellency is to combine chemical and geometric factors [1], [2]. e.g. fractal surfaces [13], functionalisation of roughened substrates with perfluoroalkyl groups [14], [15], compression of sub-micron diameter PTFE spheres [16], [17], plasma deposition in the powder regime [18], [19], [20], [21], and others [22], [23]. A new approach is described, comprising plasmachemical roughening of PTFE substrates followed by the deposition of low surface energy plasma polymer layers. X-ray photoelectron spectroscopy (XPS), atomic force microscopy (AFM), and contact angle analysis have been used to rationalise the observed enhancement in liquid repellency.

4.3.1.2. Experimental

Oxygen (BOC 99.5% purity) plasma treatments were carried out in an inductively coupled cylindrical plasma reactor on two types of PTFE substrate: flat sheet (Goodfellow), and porous film (Tetratex™ membrane 1302, pore size 0.2 μm, 50 μm thick). The reaction vessel was set up and run as described in Chapters 1 and 2.

For roughening experiments, oxygen was introduced at a constant pressure of 0.2 mbar and allowed to purge the reactor for 15 min, followed by ignition of the glow discharge. Once the treatments were complete the chamber was evacuated back down to base pressure and then brought up to atmosphere. Pulsed plasma polymerisation was carried out as described in Chapter 2.

Contact angle measurements were taken using water and decane, see Chapter 2, on: (a) the untreated sample; (b) O_2 plasma treated substrate; (c) 1H,1H,2H,2H-heptadecafluorodecyl acrylate pulsed plasma polymerised onto the substrate; and (d) O_2 plasma treated substrate followed by pulsed plasma deposition of 1H,1H,2H,2H-heptadecafluorodecyl acrylate. The surface tension of the probe liquids are given in Table 4.1.

Probe Liquid	**Surface Tension [24]**		
	γ_d	γ_p	γ
Water	22.1	50.7	72.8
Decane	23.8	0	23.8

Table 4.1 Summary of the probe liquid surface tension values.

X-ray photoelectron spectroscopy and Atomic Force Microscopy, as described in Chapter 2, were also used to analyse the treated PTFE samples.

4.3.1.3. Results and Discussion

Water has a higher surface tension compared to decane and therefore exhibits a larger contact angle on flat PTFE (γ_c = 18.5 mN m^{-1}) [25]. An increase in water contact angle is observed on going to the porous PTFE substrate [26] in accordance with the Cassie-Baxter relationship [5], Table 4.2. Whereas, the lower surface tension decane spreads out, probably as a consequence of capillary phenomenon into the large pores [27].

Oxygen plasma treatment is known to micro-roughen PTFE without perturbing its chemical identity [28]. This occurs as a consequence of ions and high energy photons from the electrical discharge impinging onto the polymer surface to generate free radical sites, which then react with atomic or molecular oxygen, followed by polymer chain scission [29]. AFM confirmed that surface roughening takes place, Figures 4.2a and 4.2b.

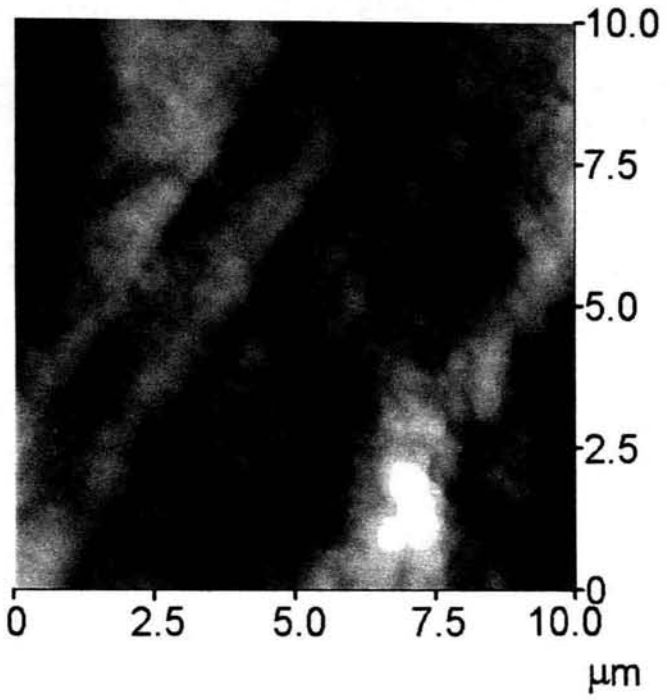

Figure 4.2a AFM image of flat untreated PTFE substrate, RMS roughness = 97 nm, z scale = 0.5 µm.

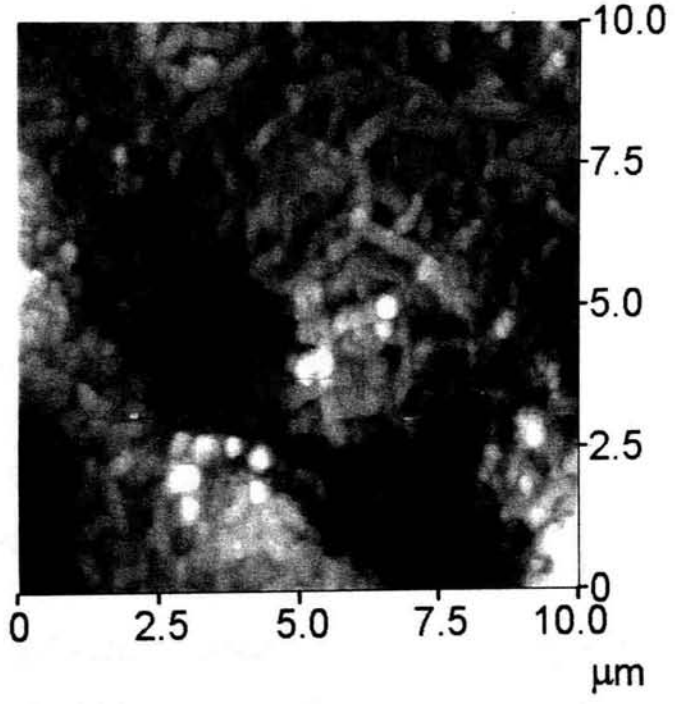

Figure 4.2b AFM image of flat PTFE following oxygen plasma treatment for 5 min at 50 W, RMS roughness = 231 nm, z scale = 2.0 µm.

Treatment	Contact Angle / °			
	Water		Decane	
	Flat	Porous	Flat	Porous
Untreated	109 ± 2	146 ± 1	46 ± 2	wets
O_2 Plasma	131 ± 4	153 ± 2	55 ± 2	wets
Plasma Polymer	131 ± 3	144 ± 1	83 ± 1	115 ± 1
O_2 Plasma + Plasma Polymer	148 ± 1	152 ± 1	92 ± 3	133 ± 2

Table 4.2 Probe liquid contact angles for flat and porous PTFE substrates (oxygen plasma treatment was carried out at 50 W for 5 min).

Whilst XPS verified the absence of any chemical change at the surface [30], since only the characteristic $\underline{C}F_2$ peak at 291.2 eV, and its corresponding Mg $K\alpha_{3,4}$ satellite peak shifted by ~9 eV towards lower binding energy [31] were present, Figure 4.3. Surface roughening produced a corresponding rise in water contact angle for both types of PTFE substrate [28], [32], [33], Figures 4.4a and 4.4b, where both electrical discharge power and duration of plasma exposure were found to be important parameters. Oxygen plasma treatment at 50 W for 5 min was chosen as the optimum conditions for the remaining studies. The increase in decane contact angle for the flat PTFE substrate suggests that sufficient surface roughening occurs in order to produce an air-PTFE composite surface which obeys the Cassie-Baxter relationship [34]. As opposed to just a mere increase in interfacial area, which according to Wenzel's relationship would have led to a decrease in contact angle [1] (since the contact angle of decane is less than 90^0 on flat PTFE), Table 4.2. In the case of decane on porous PTFE substrate, it is thought that capillary action persisted even after oxygen plasma roughening.

Deposition of 1H,1H,2H,2H-heptadecafluorodecyl acrylate pulsed plasma polymer onto the flat and porous PTFE substrates gave rise to an improvement in repellency for both probe liquids. This can be attributed to the long perfluorocarbon chains contained in the plasma polymer structure having a lower surface energy compared to PTFE, γ_c = 4.3 mN m^{-1} and 18.5 mN m^{-1} respectively, Chapter 2 [25], [35], [36]. It is of particular

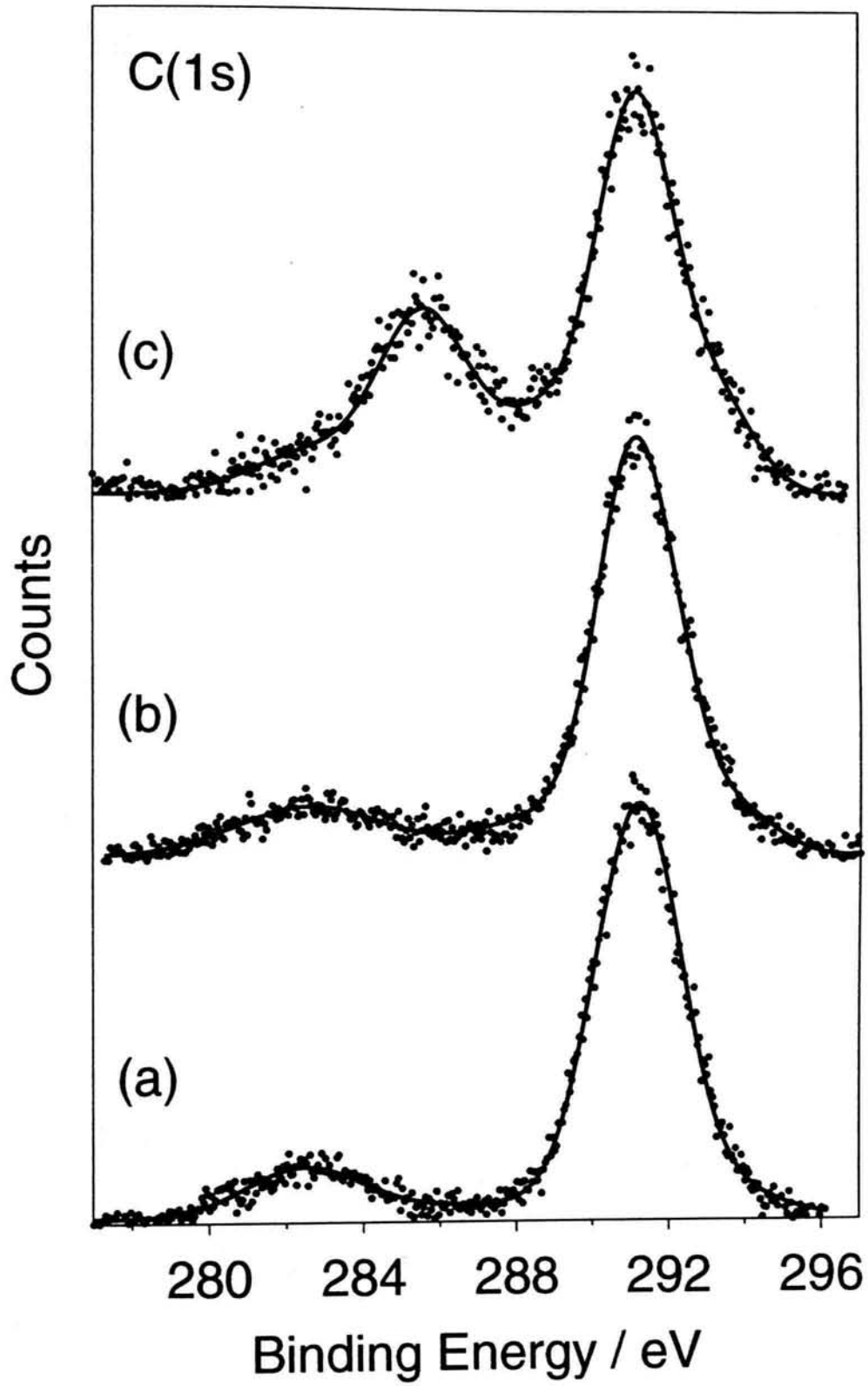

Figure 4.3 C(1s) XPS spectra for flat PTFE substrate: (a) untreated; (b) following oxygen plasma treated for 5 min at 50 W; and (c) deposition of pulsed perfluorocarbon chain acrylate onto (a).

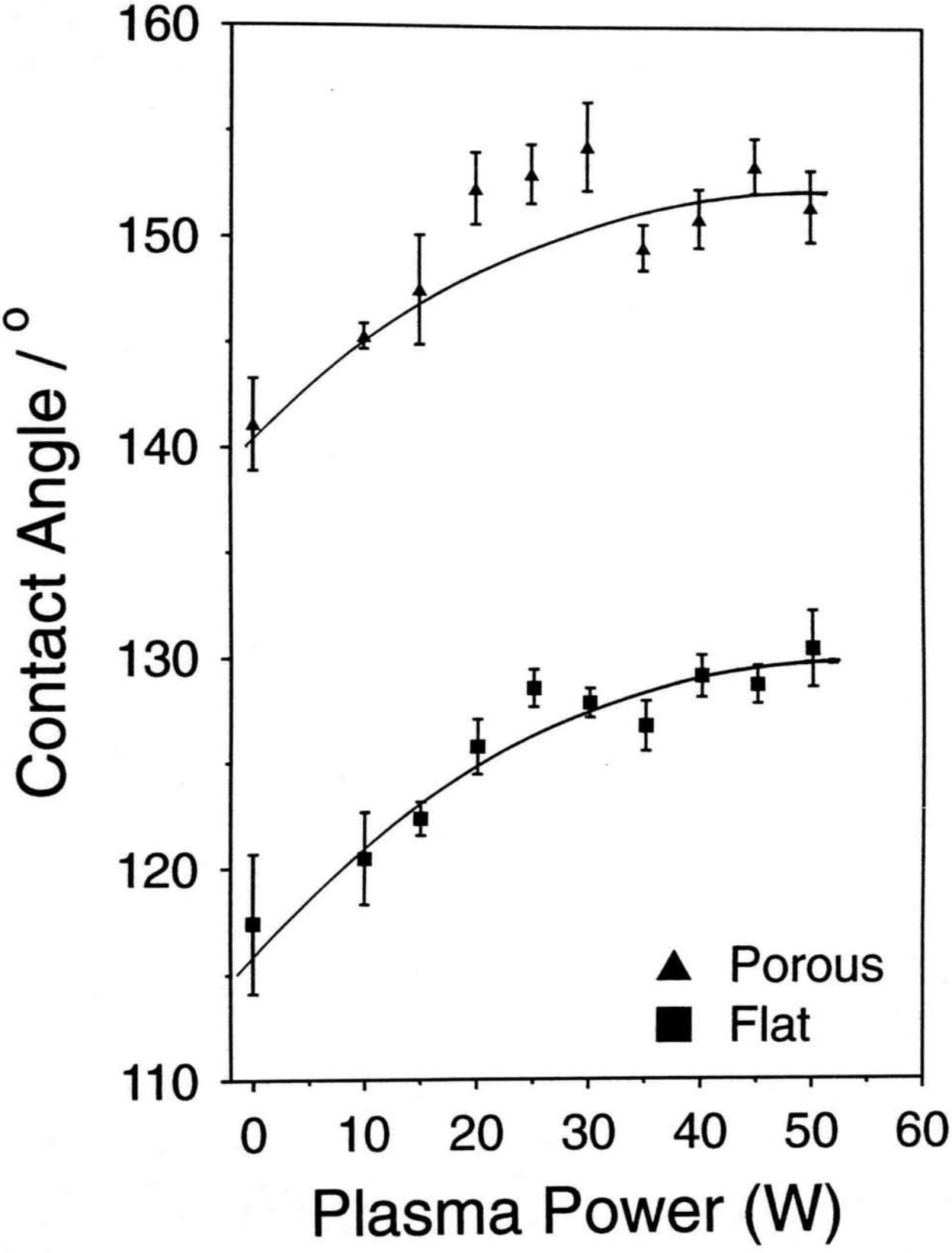

Figure 4.4a Water contact angle for flat and porous PTFE substrate following oxygen plasma treatment as a function of electrical discharge power for 2 min.

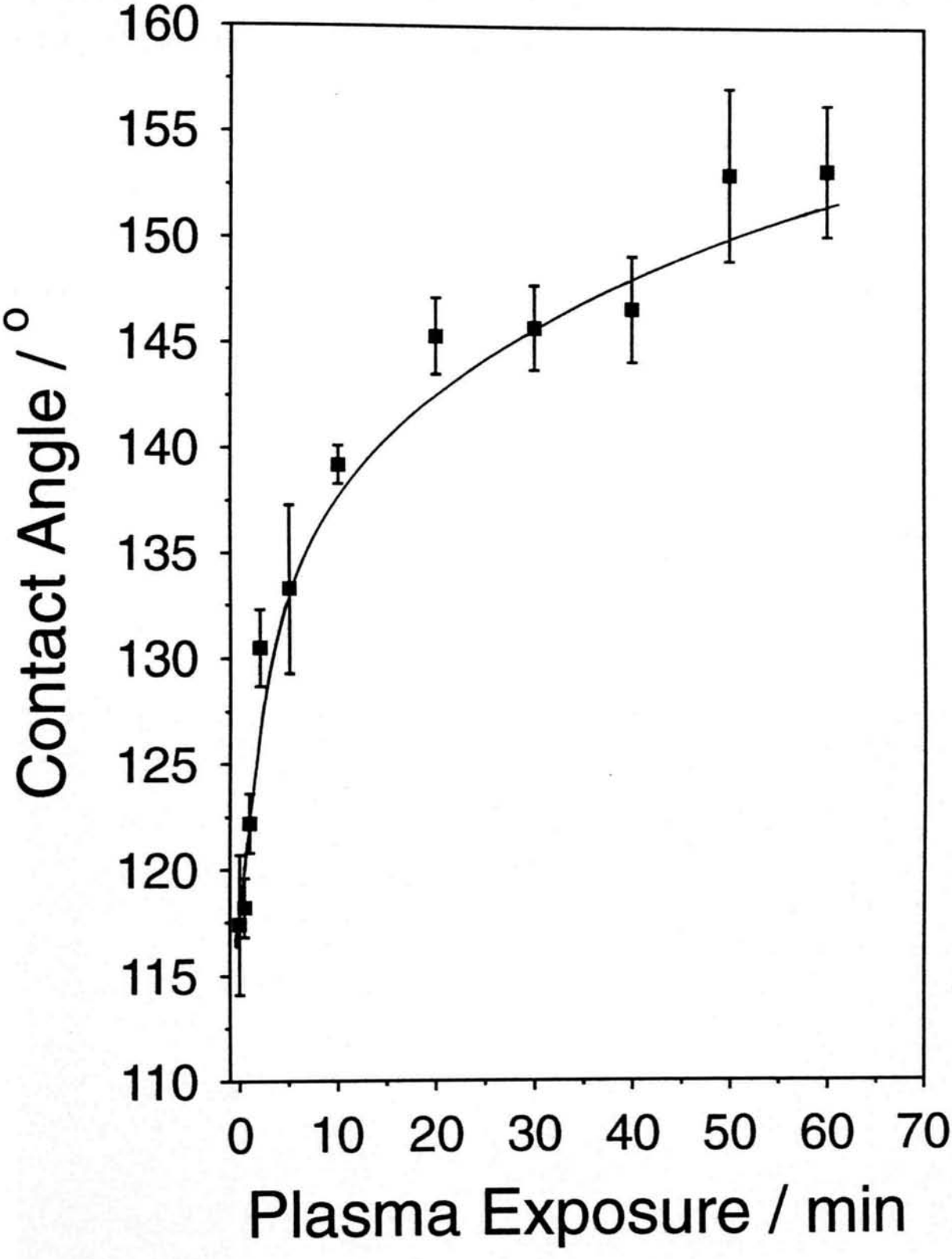

Figure 4.4b Water contact angle for flat PTFE substrate following oxygen plasma treatment as a function of treatment time at 50 W (the porous PTFE membrane was restricted to short exposures due to its fragile nature).

interest to note that the high decane contact angle measured for the coated flat PTFE surface is now sufficient to prevent capillary action into the porous substrate.

The chemical nature of the deposited plasma polymer layer was checked by XPS and the C(1s) spectra could be fitted to 7 Mg $K\alpha_{1,2}$ components [37], [38]: $\underline{C}_xH_y$ at 285.0 eV, $\underline{C}$-C(O)=O at 285.7 eV, $\underline{C}$-O/$\underline{C}$-CF_n at 286.6 eV, $\underline{C}F$ at 287.8 eV, O-$\underline{C}$=O/$\underline{C}F$-CF_n at 289.0 eV, $\underline{C}F_2$ at 291.2 eV, and $\underline{C}F_3$ at 293.3 eV (there are also corresponding Mg $K\alpha_{3,4}$ satellite peaks shifted by ~9 eV towards lower binding energy [39]). The oxygenated / hydrogenated carbon centres originate from the acrylate functionality contained in the monomer, Figure 4.3.

Oxygen plasma micro-roughening of the PTFE substrates followed by pulsed plasma polymer deposition gave rise to a further enhancement in the water and decane contact angles; with porous PTFE giving the best values, Table 4.2 and Figure 4.5.

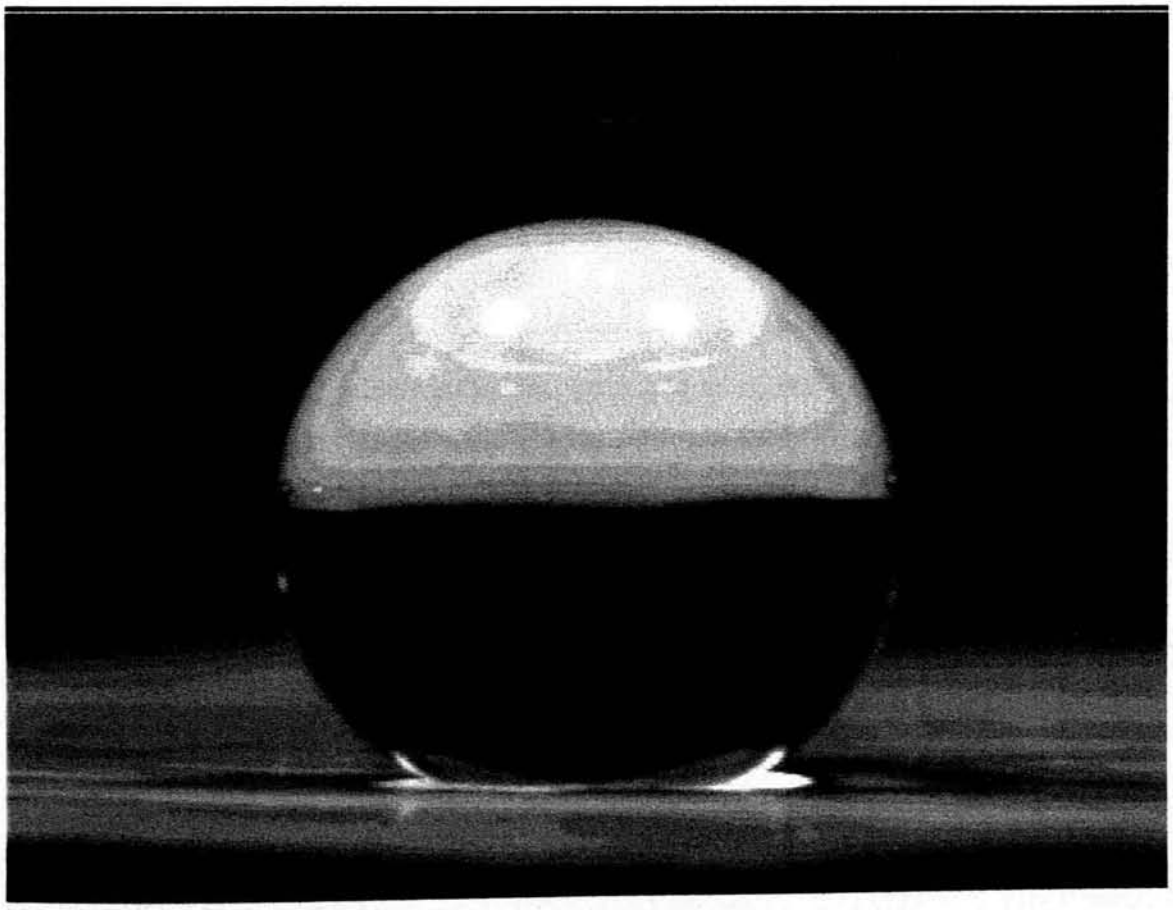

Figure 4.5 Photograph of 6 µl water droplet placed on the porous PTFE substrate which has been oxygen plasma treated for 5 min at 50 W and then coated with the long perfluorocarbon chain acrylate pulsed plasma polymer.

This can be attributed to the combined effect of the micro-roughened composite surface and the low surface energy nature of the plasma polymer layer. The observed increase in decane contact angle, despite it being less than 90^0 for the plasma polymer coated flat PTFE surface, is consistent with the Cassie-Baxter theory for composite interfaces [5], (whereas the Wenzel relationship would have predicted a decrease in contact angle [1]). Similar behaviour for low surface tension liquids has been observed upon roughening other types of substrate, which form composite interfaces [40], [41].

4.3.1.4. Conclusions

Oxygen plasma micro-roughening of non-porous and expanded PTFE substrates enhances water repellency. However, lower surface tension liquids such as decane wick out on porous PTFE as a consequence of capillary action. Deposition of a low surface energy plasma polymer coating on top of these micro-roughened PTFE surfaces further improves liquid repellency, where decane no longer penetrates into the sub-surface of the expanded PTFE substrate.

4.3.2. Water Repellent Rough Structures

4.3.2.1. Introduction

The structure chosen for the second rough surface was n-hexatriacontane which is a straight chain paraffinic molecule, exhibiting a highly crystalline form [42]. It also displays almost identical properties to high density polyethylene [43], [44], [45], such as atomic, electronic and valence structure [46] and ultraviolet absorption characteristics [47]. Previously electron microscopy, optical microscopy [48], X-ray diffraction and atomic force microscopy [49] have been used to study n-hexatriacontane crystals.

It was believed that CF_4 plasma treatment of the crystal structures would both roughen the surface further and incorporate fluorine functionalities to lower the surface energy. Experiments were carried out to see if the level of roughness would exceed that of the PTFE, and hence generate a more repellent surface.